Received: 13 June 2022 | Revised: 3 January 2023 | Accepted: 3 January 2023

DOI: 10.1111/joa.13826

Journal of Anatomy ANATOMICAL SOCIETY WILEY

ORIGINAL ARTICLE

Ecomorphological patterns in trigeminal canal branching among sauropsids reveal sensory shift in suchians

Emily J. Lessner[1] | Kathleen N. Dollman[2] | James M. Clark[3] | Xing Xu[4,5] | Casey M. Holliday[1]

[1]Department of Pathology and Anatomical Sciences, University of Missouri, Columbia, Missouri, USA

[2]European Synchrotron and Radiation Facility, Grenoble, France

[3]Department of Biological Sciences, George Washington University, Washington, District of Columbia, USA

[4]Centre for Vertebrate Evolutionary Biology, Yunnan University, Kunming, China

[5]Institute of Vertebrate Paleontology and Paleoanthropology, Chinese Academy of Sciences, Beijing, China

Correspondence
Emily J. Lessner, Department of Pathology and Anatomical Sciences, University of Missouri, Columbia, MO 65212, USA.
Email: ejlessner@mail.missouri.edu

Funding information
Evolving Earth Foundation; National Natural Science Foundation of China, Grant/Award Number: 41688103 and 42288201; National Science Foundation, Grant/Award Number: EAR 1631684, EAR 1636753, EAR 1762458 and IOS 1457319; Society of Vertebrate Paleontology; University of Missouri Life Sciences Fellowship Program; Missouri Research Board; Department of Pathology and Anatomical Sciences, University of Missouri School of Medicine

Abstract

The vertebrate trigeminal nerve is the primary mediator of somatosensory information from nerve endings across the face, extending nerve branches through bony canals in the face and mandibles, terminating in sensory receptors. Reptiles evolved several extreme forms of cranial somatosensation in which enhanced trigeminal tissues are present in species engaging in unique mechanosensory behaviors. However, morphology varies by clade and ecology among reptiles. Few lineages approach the extreme degree of tactile somatosensation possessed by crocodylians, the only remaining members of a clade that underwent an ecological transition from the terrestrial to semiaquatic habitat, also evolving a specialized trigeminal system. It remains to be understood how trigeminal osteological correlates inform how adaptations for enhanced cranial sensation evolved in crocodylians. Here we identify an increase in sensory abilities in Early Jurassic crocodylomorphs, preceding the transitions to a semiaquatic habitat. Through quantification of trigeminal neurovascular canal branching patterns in an extant phylogenetic bracket we quantify and identify morphologies associated with sensory behaviors in representative fossil taxa, we find stepwise progression of increasing neurovascular canal density, complexity, and distribution from the primitive archosaurian to the derived crocodilian condition. Model-based inferences of sensory ecologies tested on quantified morphologies of extant taxa with known sensory behaviors indicate a parallel increase in sensory abilities among pseudosuchians. These findings establish patterns of reptile trigeminal ecomorphology, revealing evolutionary patterns of somatosensory ecology.

KEYWORDS
crocodyliforms, ecomorphology, somatosensation, trigeminal

1 | INTRODUCTION

Numerous key innovations in early vertebrate evolution led to the emergence of the vertebrate head as an integrated organ system responsible for receipt, interpretation, and response to various external stimuli (Gans & Northcutt, 1983). As a result, the trigeminal nerve (CN V) is the primary somatosensory nerve of the head, mediating sensory perception as the organism engages in daily activities, danger avoidance, food localization and capture, and other feeding behaviors. As such, the trigeminal nerve and its receptors convey sensations of touch, proprioception, temperature, pain, and itch from the integument of the head.

The trigeminal system (detailed below), though conserved in general form, is diverse among vertebrates, particularly sauropsids (i.e., lizards, snakes, crocodilians, birds), some of which evolved extreme forms of cranial somatosensation. The most derived forms, such as touch-sensitive crocodilians and probe-feeding birds, optimize the mechanosensitive portion of their trigeminal sensory system, possessing unique cranial morphologies adapted for mediating prey acquisition via tactile somatosensory input (Cunningham et al., 2013; Leitch & Catania, 2012).

It remains to be understood how these adaptations for cranial sensation evolved among different clades of sauropsids, including specific lineages of lepidosaurs, crocodylians, and birds. Few neontological studies explore patterns of trigeminal nerve diversity among sauropsids (e.g., Crole & Soley, 2014; Cunningham et al., 2013; du Toit et al., 2022; George & Holliday, 2013; Gutiérrez-Ibáñez et al., 2009; Leitch & Catania, 2012; Lessner, 2020). Similarly, few paleontological studies use osteological structures to predict nervous tissue anatomy, limiting investigation to small ranges of extinct dinosaur and crocodylian species. However, these hypotheses require thorough testing using modern imaging, morphometrics, and phylogenetic comparative methods. Overall, we still lack consistent anatomical and morphometric means of comparing relative sensation across lineages of reptiles, and the origins of extreme forms of sensation in the clade remain largely unexplored.

This research identifies patterns in form and function of the sauropsid trigeminal system, focusing on trigeminal nerve-mediated tactile sensation of the lower jaws. To discriminate between organisms of different sensory abilities, we quantified and compared complex branching patterns of mandibular (inferior alveolar) neurovascular canals terminating in tactile sensory receptors (Figure 1). This expands the work of Lessner (2020), which introduced a method to quantify canals and hypothesized the method could discriminate between organisms of different sensory abilities and ecologies. Using a sample of extant reptiles with known tactile sensory abilities and ecologies, we build predictive, statistical models for hypothesizing sensory ability across the fossil record to better identify evolutionary transitions in lineages of sauropsids and other vertebrates. The models use multiple variables, several body size-independent, increasing predictive capacity and allowing ecological predictions to be drawn from isolated dentaries and fragmentary specimens. We illustrate these approaches by exploring the fossil record of crocodyliforms and their ancestors to test for when their derived sense of trigeminal nerve-innervated somatosensation evolved.

1.1 | Trigeminal anatomy and physiology in sauropsids

In vertebrates, the trigeminal nerve follows a largely conserved path from its origin in the hindbrain to nerve endings across the face (see Holliday & Witmer, 2007 for a detailed comparative summary). The trigeminal nerve and associated neurovasculature leave osteological correlates in the form of foramina, depressions, grooves, and canals which can be traced along this pathway through the skull. An in-depth understanding of these paths and their osteological correlates allow for better predictions of soft tissues in fossil organisms.

In sauropsids, the trigeminal nerve courses from sensory and motor nuclei in the mid- and hindbrain, exiting the brain through roots extending from the pons. The cell bodies of the sensory root form two trigeminal ganglia (i.e., profundal and Gasserian), which are variably fused (into a single "trigeminal ganglion") and located alongside the braincase with variable bony enclosure (Barbas-Henry & Lohman, 1986; Holliday & Witmer, 2009; Hopson, 1979; Oelrich, 1956; Willard, 1915; Witmer et al., 2008). Three divisions extend rostrally from the ganglion. The ophthalmic and maxillary divisions of the trigeminal nerve transmit sensory signals from the nasal cavity, orbit, sclera, oral cavity, palate, and the upper jaw, whereas the mandibular division transmits both motor and sensory signals to and from the lower jaw. Of these three trigeminal divisions, the mandibular division has the least complicated dermatome as it only innervates the lower jaw, tongue, and teeth, thus offering a cleaner signal of cranial somatosensation than the other nerve divisions. So, here we focus on the mandibular division as a means for understanding evolution of sauropsid sensory reception. As the mandibular nerve enters the Meckelian fossa of the mandibles, medial and oral intermandibular branches extend to innervate epithelium of the mouth, dental lamina, and integument before the mandibular nerve enters the dentary (Abdel-Kader et al., 2011). Numerous lingual, mucosal, and dental branches extend from the intermandibular and rostral mandibular (inferior alveolar) nerves to their terminations in the oral cavity, and foramina in the dentary transmit cutaneous branches to their terminations in the integument of the rostral mandibles.

Sensory receptors are present at the afferent terminations of the trigeminal nerve. In lepidosaurs, integumentary sensory receptors are well known and morphology and distribution are extensively studied (e.g., Ananjeva et al., 1991; Breyer, 1929; Grace et al., 1999; Hiller, 1968; Jackson, 1977; Landmann, 1975; Matveyeva & Ananjeva, 1995; Orejas-Miranda et al., 1977; Schmidt, 1920; Sherbrooke & Nagle, 1996; Young & Wallach, 1998; etc.). Function is less well known, but Hiller (1978) confirmed some receptors served as a mechanosensitive function. Regardless, among squamates, vision and chemosensation are prioritized while navigating environments (i.e., feeding, mate identification, maneuvering) and facilitated through alternative cranial nerves (Cooper, 1994; Schwenk, 1994). Trigeminal sense organs in extant archosaurs (e.g., birds and crocodilians) are well understood, especially in taxa considered to have highly sensitive faces. Extant crocodylians are known for having highly sensitive snouts covered with integumentary sensory organs (ISOs) In *Alligator mississippiensis*, this sensory system is specialized for a semiaquatic lifestyle, with the ability to sense minute changes in water pressure, temperature, and pH (Di-Poï & Milinkovitch, 2013) and optimized to receive and forage using mechanosensory cues of prey items (Leitch & Catania, 2012). Some extant birds are also specialized for trigeminal nerve-innervated somatosensation, also optimizing structures which receive mechanosensory cues from potential food (Cunningham et al., 2013; du Toit et al., 2022), whereas others rely more heavily on visual cues (Martin, 2007; Martin & Coetzee, 2004). Trigeminal-supplied bill tip organs are known from multiple families of probe- and tactile-foraging (i.e., dabbling) birds (e.g., Baumel & Witmer, 1993; Berkhoudt, 1980; Cunningham et al., 2010). The cell types responsible for mechanical sensation reception are morphologically similar among sauropsids as well (Baumel & Witmer, 1993; Landmann, 1975; Leitch & Catania, 2012; vonDüring, 1973).

Learning whether these taxa are allocating more branches or neurovascular tissue to the rostrum will reveal the functional significance and evolutionary origins of these changes. Understanding homology allows for an understanding of the diversity of forms we see across extant sauropsids.

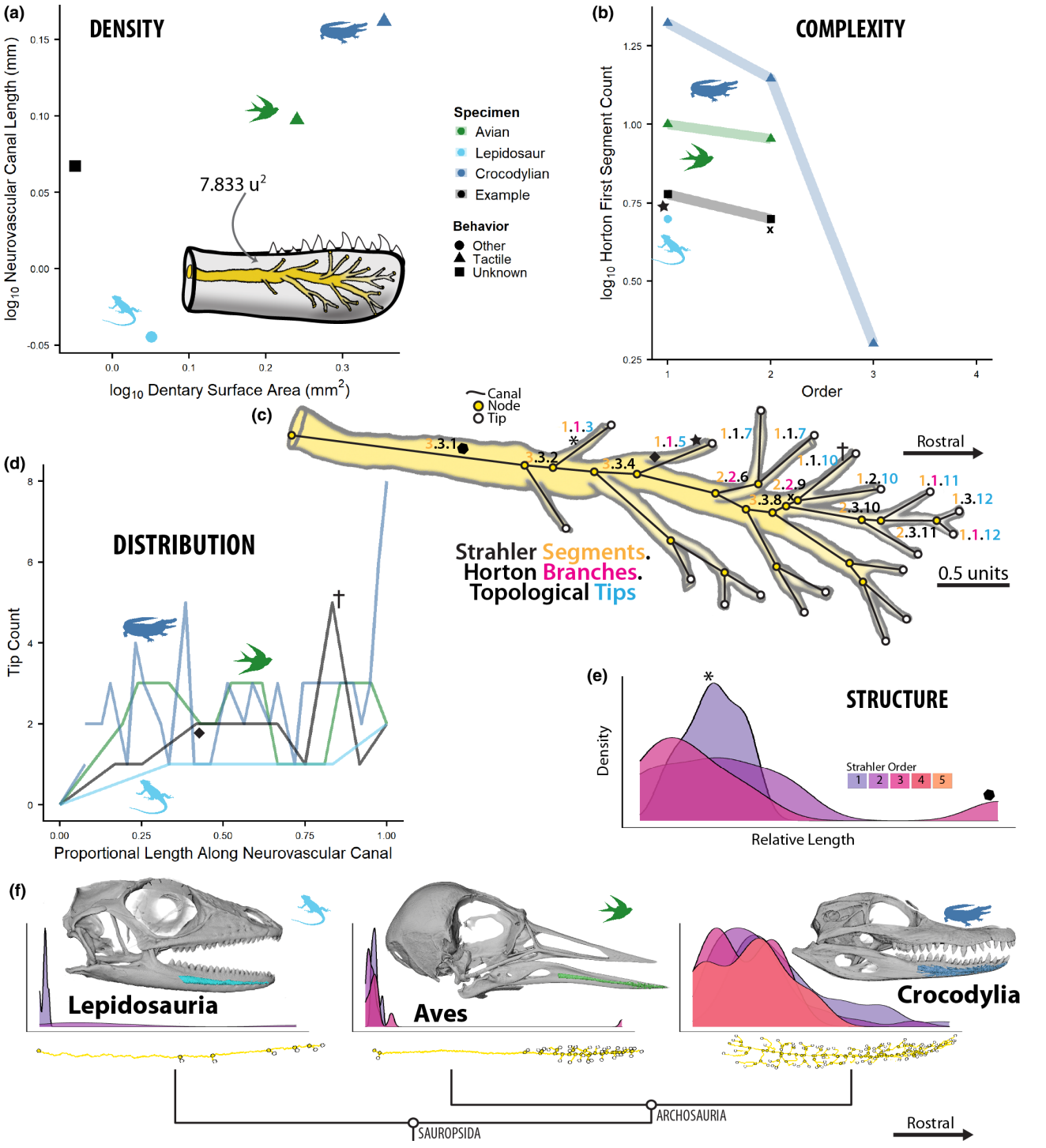

FIGURE 1 Branching quantification methods with an example canal (c) and plots of dendritic density (a), branch complexity (b), branch distribution (d), and segment structure (e) including representative taxa (f). Symbols in (c) correspond with example data on plots (b, d, e)

1.2 | Osteological correlates and inferences of sensation

Bony features indicative of soft tissue counterparts, known as osteological correlates, may be used to develop inferences of behavior and ecology in extinct organisms from fossil material. For inferences to be well supported, osteological and associated soft tissue data must be collected from a sample of extant organisms. Only when a causal relationship is established between bony and soft tissue morphology and behavior in extant organisms may inferences of soft tissue and evolutionary hypotheses be made for extinct organisms (Witmer, 1995). The trigeminal system has similar potential. Thus, to explore the potential for specialized trigeminal nerve-innervated sensation among members of Archosauria,

osteological correlates of trigeminal soft tissues must be validated in an extant phylogenetic bracket of sauropsids. Using data collected in extant sauropsids, this project establishes a sound osteological correlate for trigeminal soft tissues in sauropsids. The mandibular (inferior alveolar) canal morphology is determined a useful correlate for prediction of soft tissues, their function, and how these tie with behavior and ecology.

Osteological correlates of nerves were used to hypothesize cranial sensation in non-avian dinosaurs (Barker et al., 2017; Carr et al., 2017; Ibrahim et al., 2014; Rothschild & Naples, 2017). However, only the absolute presence of foramina was used as a proxy for what was considered to be extreme, "crocodile-like" cranial sensation. Thus, these approaches are lacking comparison with an extant phylogenetic bracket and the hypotheses remain speculative; they were based solely on the presence of foramina or canals, neither using morphometric approaches nor corroborating their interpretations with quantitative analyses of trigeminal ganglia, neurovascular canals, or more proximal foramina.

Meanwhile, we know more about the trigeminal system in alligators, crocodyliforms, and their suchian ancestors. Sensory organs in crocodylians are receptive to prey movement, used for behaviors such as prey capture and maneuvering (Leitch & Catania, 2012), and the foraminous jaws representative of this system were hypothesized to only be present in semiaquatic members of the clade after the Early Jurassic (Soares, 2002). Quantitative analyses of *Alligator mississippiensis* head length, brain size, and trigeminal nerve size confirmed trigeminal ganglion size as an informative metric for trigeminal nerve size in crocodyliforms and hypothesized that the feature was an informative proxy for sensitivity and that the unique system seen in extant crocodylians originated along the eusuchian line (George & Holliday, 2013). Though extant crocodylians are conservative in morphology and ecology, occupying similar semiaquatic niches, extinct suchians exhibited diverse forms, and occupied terrestrial to aquatic habitats (Brusatte et al., 2010; Sellers et al., 2022; Wilberg et al., 2019), likely requiring differing sensory abilities to navigate their environments. Inferences in extinct species are expected to show a trend from less to more trigeminal sensation across suchians because of a trend toward a semiaquatic lifestyle.

1.3 | Ecological, behavioral, and morphological transitions in sensation

Ecological transitions exert selective pressures on morphological features and behaviors, and because sensory systems provide adaptive advantages (Leitch & Catania, 2012; Ryan, 1990; Yoshizawa & Jeffery, 2011), they are subject to changes in form and function over ecological transitions. Across sauropsid evolutionary history, numerous transitions occurred in different linages affecting sensation, including edentulism, semiaquatic lifestyles, limblessness, flight, and fossoriality, among others. For example, transitions to limblessness often occur in concert with eye reduction and enhanced chemosensation, whereas the transition to flight is tied with increased visual and spatial perception abilities (Alonso et al., 2004; Gans, 1975). The environment is one factor affecting signal receipt and transmission and therefore sensation. As such, organisms in different environments tend to possess specialized sensory organs. This is well documented in multiple cases: electrosensitivity is more prominent in aquatic environments because of the conductivity of water; vision is often exchanged for other modalities in low light environments; birds exhibit higher visual acuity than non-flighted animals, etc. (Martin, 2012; Stevens, 2013). Sensory adaptations are frequently noted among animals inhabiting aquatic environments (e.g., crocodylian mechanoreceptors, olfactory system regression in aquatic snakes) (Thewissen & Nummela, 2008). Within Lepidosauria, at least 14 clades contain members that independently transitioned to fully aquatic ecologies, within bird-line archosaurs (i.e., Avemetatarsalia) numerous avian taxa have aquatic ecologies, and within crocodylian-line archosaurs (i.e., Suchia), at least three clades contain members that independently transitioned to fully aquatic ecologies (Thewissen & Nummela, 2008; Wilberg et al., 2019).

Although special senses (i.e., vision, hearing, smell, taste, balance) are commonly followed across macroevolutionary transitions (e.g., Angielczyk & Schmitz, 2014; Bronzati et al., 2021; MacIver et al., 2017; Neenan et al., 2017; Schmitz & Motani, 2011), research on trigeminal-specific adaptations is limited to single clade or species-specific investigations.

Similarly, it is expected dermatomes are more richly innervated in taxa feeding in aquatic habitats than non-aquatic taxa because previously observed aquatic taxa (e.g., crocodylians, ducks, probing birds) exhibit high densities of trigeminal soft tissue structures indicative of their trigeminal abilities and use specialized, trigeminal-innervated structures to acquire food (Cunningham et al., 2013; du Toit et al., 2022; Leitch & Catania, 2012).

Suchia, the lineage of fossil archosaurs including extant crocodylians, proves a useful group in which to evaluate hypotheses of evolving trigeminal tissues with transitions in ecology. Osteological correlates in suchians are robust and habitat shifts are well known (Wilberg et al., 2019). Basal suchians occupied terrestrial habitats from their origins in the Early Triassic (+245 Ma) (Nesbitt, 2011) and crocodylomorphs began to invade aquatic habitats after the Triassic-Jurassic boundary (201.3 Ma, Wilberg et al., 2019). It is expected that this habitat transition was accompanied by changes in sensory systems toward the extant condition including an expanded trigeminal ganglion (George & Holliday, 2013; Lessner et al., 2022), numerous ISOs, and use of innervated jaws for prey capture and maneuvering (Leitch & Catania, 2012) which may be detected through investigation of trigeminal osteological correlates. It was hypothesized enhanced, trigeminal-innervated somatosensory systems of extant crocodylians originated in the Early Jurassic based on the presence of rostral foramina (Soares, 2002), and other trigeminal osteological correlates were suggested as proxies for cranial sensation in early crocodyliforms (George & Holliday, 2013). However, these studies

were limited in quantitative analysis and sample size, and patterns and processes underlying this major transformation in vertebrate sensory evolution and habitat remain untested. Because sensory systems commonly change with habitat shifts (Thewissen & Nummela, 2008) and we see a highly specialized extant condition, we expect the trigeminal system also coevolved with the transition to aquatic environments and ambush predation.

The following documents variation in trigeminal-nerve structures in living sauropsids through quantitative comparison of morphology of the mandibular (inferior alveolar) canal and sensory behaviors. This creates a robust extant phylogenetic bracket for statistical inferences of sensory behaviors from osteological correlates in extinct animals and is used here to identify patterns in the evolution of the derived condition present in extant crocodylians.

2 | MATERIALS AND METHODS

2.1 | Specimen selection and categorization

Specimen selection was based both on specimen and data availability from University of Missouri and other natural history collections and on organism ecology. Among the extant sauropsids, we sampled broadly across the avian, lepidosaurian, and crocodylian clades. All extant crocodylians are known to engage in specialized trigeminal tactile-sensory behaviors (i.e., foraging using solely mechanosensory cues; Leitch & Catania, 2012). No such behaviors are identified among lepidosaurs, which are known to prioritize vision and chemosensation when navigating their environments (Cooper, 1994; Schwenk, 1994). Extant avians however are more variable, so taxa representative of specialized trigeminal tactile-sensory behaviors (i.e., foraging via dabbling or probing, using solely mechanosensory cues; Cunningham et al., 2013; du Toit et al., 2022) and non-representatives (i.e., visual-foragers; Martin, 2007; Martin & Coetzee, 2004) were sampled. For fossil specimens, the crocodylian line of archosaurs were targeted because of the condition of extant crocodilians. Suchians were sampled broadly from the stem of Crocodylia based on availability, scanning suitability, and completeness. (Table 1).

2.2 | Whole-mount nerve staining

Whole-mount nerve staining (Figure 2) provides an alternative method of nerve visualization when high-resolution, contrast-enhanced computed tomography (CT) scanning is not possible. Specimens were fixed in 10% neutral buffered formalin, immersed in distilled water then hydrogen peroxide, and macerated in a sodium borate-trypsin solution as in Filipski and Wilson (1986, see for complete protocol). This was followed by immersion in water, ethanol, Sudan Black B stain, and glycerol. A Nikon Digital Sight U2/L2 camera and NIS-Elements F v 4.30.01 software were used to photograph specimens through a Nikon SMZ100 microscope.

2.3 | CT scanning and segmentation

In all, 35 extant specimens (8 avians, 13 crocodylians, and 14 lepidosaurs) and 11 fossil specimens (1 archosauriform and 10 non-crocodylian suchians) (Figure 3) underwent CT scanning at various resolutions allowing for visualization of bone and neurovascular canals (Figure 4). Neurovascular canal contents were verified and compared with canal size in representative extant taxa using contrast-enhanced (Gignac et al., 2016) CT scans (Figures 3 and 4; Table 1). These specimens were immersed in I_2KI (4.1%–12.3% w/v) for varying durations. Duration and stain concentration were dependent on specimen size and robusticity; large specimens required higher stain concentrations and durations, whereas small (especially avian) specimens required the opposite (Table S1). Scan data were imported as DICOM and TIFF files into Avizo v. 9 (Thermo Fisher Scientific) for segmentation and ImageJ (Schneider et al., 2012) for analysis. Magic wand and paint-brush tools with interpolation were used to segment rostral dentaries (the portion rostral to the complete enclosure of the mandibular canal by bone) and neurovascular canals within the rostral dentaries. The caudal, or proximal, extent of the canal quantified in this project is marked by the complete enclosure of the mandibular neurovasculature by the dentary.

2.4 | 3D model measurement and processing

Skull width was collected using the "Measure: 2D length" tool, and cross-sectional areas (CSAs) were collected in Avizo using the "Material Statistics: Area per slice" module or in Image J. Dentary surface area was collected (of the lateral, integumentary, foraminiferous portion) using the surface editor and "Surface Area Statistics" module. Neurovascular canals were reconstructed using the "Centerline Tree" module, annotated with topological, Strahler, and Horton orders, and these values (segment lengths and orders) collected in attribute graph .xlsx files as described by Lessner (2020). To assign topological orders, the origin segment (opening of the mandibular [inferior alveolar] canal) was designated order 1 and at each division, subsequent segment orders increase by 1 (Figure 1c). This allows identification of a main canal, which is the set of segments from the origin to the segment of highest topological order (with the longest total length). Strahler orders are designated by assigning all terminal segments an order of 1, and then at each junction if two like segments converge, order increases by one, otherwise the following segment takes the higher order of the two converging segments (Figure 1c). To assign Horton order, the highest Strahler order is assigned to each segment of the main canal identified by the topological method. Lone terminal segments from the main canal are assigned to order 1, and for paired terminal segments elsewhere, the shorter segment is assigned to order 1. To designate orders to branches, end-to-end segments are assigned order 2 if only sharing junctions with first-order segments and assigned order 3 if sharing junctions with first and second-order segments (Figure 1c). Orders of the first segment of a branch from the main canal (Horton first segment orders) were collected as well.

TABLE 1 Specimens and prediction results (fossil specimens shaded)

Specimen	Clade	Ecology (literature citations below)	% Tactile: topological tips	Density metrics and topological COM	Strahler segments	Horton first segments	% Tactile: mean segment length (a)	% Tactile: median segment lengths	% Tactile: mode segment lengths
*Alle alle**	Avian	Non-tactile (1)	10	Non-tactile	Non-tactile	Non-tactile	0	0	0
*Alligator mississippiensis**	Crocodylian	Tactile (2)	80	Tactile	Tactile	Tactile	100 (67)	100	100
*Alligator mississippiensis***	Crocodylian	Tactile (2)	100	Tactile	Tactile	Tactile	100 (67)	100	100
*Anas platyrhynchos***	Avian	Tactile (3)	80	Tactile	Tactile	Tactile	100 (67)	100	67
*Anolis sagrei**	Lepidosaur	Non-tactile (4)	0	Non-tactile	Non-tactile	Non-tactile	0 (0)	0	0
Araripesuchus gomesii	Crocodyliform	Unknown	50	Tactile	Tactile	Tactile	67 (67)	33	33
Arenaria melanocephala	Avian	Tactile (3)	50	Tactile	Non-tactile	Neutral	67 (67)	100	100
*Brookesia**	Lepidosaur	Non-tactile (4)	0	Non-tactile	Non-tactile	Tactile	0 (0)	0	0
*Crocodylus johnstoni**	Crocodylian	Tactile (2)	90	Tactile	Tactile	Tactile	100 (67)	100	100
*Crocodylus johnstoni***	Crocodylian	Tactile (2)	70	Tactile	Tactile	Tactile	100 (67)	100	67
Crocodylus moreletii	Crocodylian	Tactile (2)	90	Tactile	Tactile	Tactile	100 (67)	100	100
*Crocodylus porosus**	Crocodylian	Tactile (2)	100	Tactile	Tactile	Tactile	100 (67)	100	100
Caiman crocodilus	Crocodylian	Tactile (2)	100	Tactile	Tactile	Tactile	100 (100)	100	100
*Crotaphytus collaris**	Lepidosaur	Non-tactile (4)	0	Non-tactile	Non-tactile	Non-tactile	0 (0)	0	0
*Ctenosaura pectinata**	Lepidosaur	Non-tactile (4)	0	Non-tactile	Non-tactile	Non-tactile	0 (0)	0	0
*Dracaena guianensis**	Lepidosaur	Non-tactile (4)	0	Non-tactile	Non-tactile	Non-tactile	0 (0)	0	0
*Eremias arguta**	Lepidosaur	Non-tactile (4)	10	Non-tactile	Non-tactile	Non-tactile	0 (0)	0	0
*Fulica americana**	Avian	Non-tactile (1)	40	Tactile	Tactile	Non-tactile	0 (33)	33	33
Junggarsuchus sloani	Crocodylomorph	Unknown	30	Non-tactile	Non-tactile	Non-tactile	33 (33)	0	33
Litargosuchus leptorhynchus	Crocodylomorph	Unknown	50	Tactile	Non-tactile	Neutral	33 (67)	67	100
Longosuchus meadi	Suchian	Unknown	50	Non-tactile	Tactile	Neutral	33	67	67
Macelognathus vagans	Crocodylomorph	Unknown	60	Tactile	Tactile	Neutral	33	0	33
Mecistops cataphractus	Crocodylian	Tactile (2)	100	Tactile	Tactile	Tactile	100 (100)	100	100
Nominosuchus	Crocodyliform	Unknown	40	Tactile	Non-tactile	Neutral	33 (67)	0	0
Orthosuchus stormbergi	Crocodyliform	Unknown	60	Tactile	Tactile	Neutral	100 (100)	67	67
*Osteolaemus tetraspis**	Crocodylian	Tactile (2)	100	Tactile	Tactile	Tactile	100 (67)	100	100
*Osteolaemus tetraspis***	Crocodylian	Tactile (2)	100	Tactile	Tactile	Tactile	100 (100)	100	100
*Paleosuchus palpebrosus**	Crocodylian	Tactile (2)	80	Tactile	Tactile	Tactile	100 (100)	67	67
*Pandion haliaetus**	Avian	Non-tactile (1)	20	Non-tactile	Non-tactile	Non-tactile	0 (67)	33	67
Pelagosaurus typus	Crocodyliform	Unknown	30	Non-tactile	Tactile	Neutral	100	100	100

TABLE 1 (Continued)

Specimen	Clade	Ecology (literature citations below)	% Tactile: topological tips	Density metrics and topological COM	Strahler segments	Horton first segments	% Tactile: mean segment length (a)	% Tactile: median segment lengths	% Tactile: mode segment lengths
*Phasianus colchicus**	Avian	Non-tactile (1)	40	Non-tactile	Non-tactile	Non-tactile	33 (67)	0	33
*Physignathus cocincinus**	Lepidosaur	Non-tactile (4)	0	Non-tactile	Non-tactile	Non-tactile	0 (50)	0	0
*Pogona vitticeps**	Lepidosaur	Non-tactile (4)	0	Non-tactile	Non-tactile	Non-tactile	0 (50)	0	0
Protosuchus haughtoni	Crocodyliform	Unknown	80	Tactile	Tactile	Neutral	33 (100)	33	33
*Psittacus erithacus**	Avian	Tactile (3)	50	Tactile	Tactile	Tactile	100 (100)	67	100
*Scolopax rusticola***	Avian	Tactile (3)	100	Tactile	Tactile	Tactile	100 (100)	100	100
Simosuchus clarki	Crocodyliform	Unknown	60	Tactile	Tactile	Tactile	100 (67)	0	33
*Sphaerodactylus caicosensis**	Lepidosaur	Non-tactile (4)	0	Non-tactile	Non-tactile	Non-tactile	0 (0)	50	0
*Sphenodon punctatus**	Lepidosaur	Non-tactile (4)	10	Non-tactile	Non-tactile	Non-tactile	0 (0)	0	0
*Tomistoma schlegelii**	Crocodylian	Tactile (2)	100	Tactile	Tactile	Tactile	100 (100)	100	100
*Tomistoma schlegelii***	Crocodylian	Tactile (2)	100	Tactile	Tactile	Tactile	100 (100)	100	100
Trilophosaurus buettneri	Archosauromorph	Unknown	20	Non-tactile	Non-tactile	Neutral	33	33	33
*Trioceros bitaeniatus**	Lepidosaur	Non-tactile (4)	0	Non-tactile	Non-tactile	Non-tactile	0 (50)	50	0
*Uromastyx geyri**	Lepidosaur	Non-tactile (4)	0	Non-tactile	Non-tactile	Non-tactile	0 (0)	0	0
*Varanus exanthematicus**	Lepidosaur	Non-tactile (4)	10	Non-tactile	Non-tactile	Non-tactile	0 (50)	0	0
*Varanus salvator**	Lepidosaur	Non-tactile (4)	0	Non-tactile	Non-tactile	Non-tactile	0 (0)	0	0

Note: (1) Martin and Coetzee (2004), Martin (2007). (2) Leitch and Catania (2012), Di-Poï and Milinkovitch (2013), Grap et al. (2020). (3) Cunningham et al. (2013). (4) Cooper (1994), Schwenk (1994).
(*) Contrast-enhanced scan for soft-tissue verification. (**) Soft-tissue verified in contrast-enhanced scan of alternate specimen. (a) Values when skull width is used as a proxy for size.

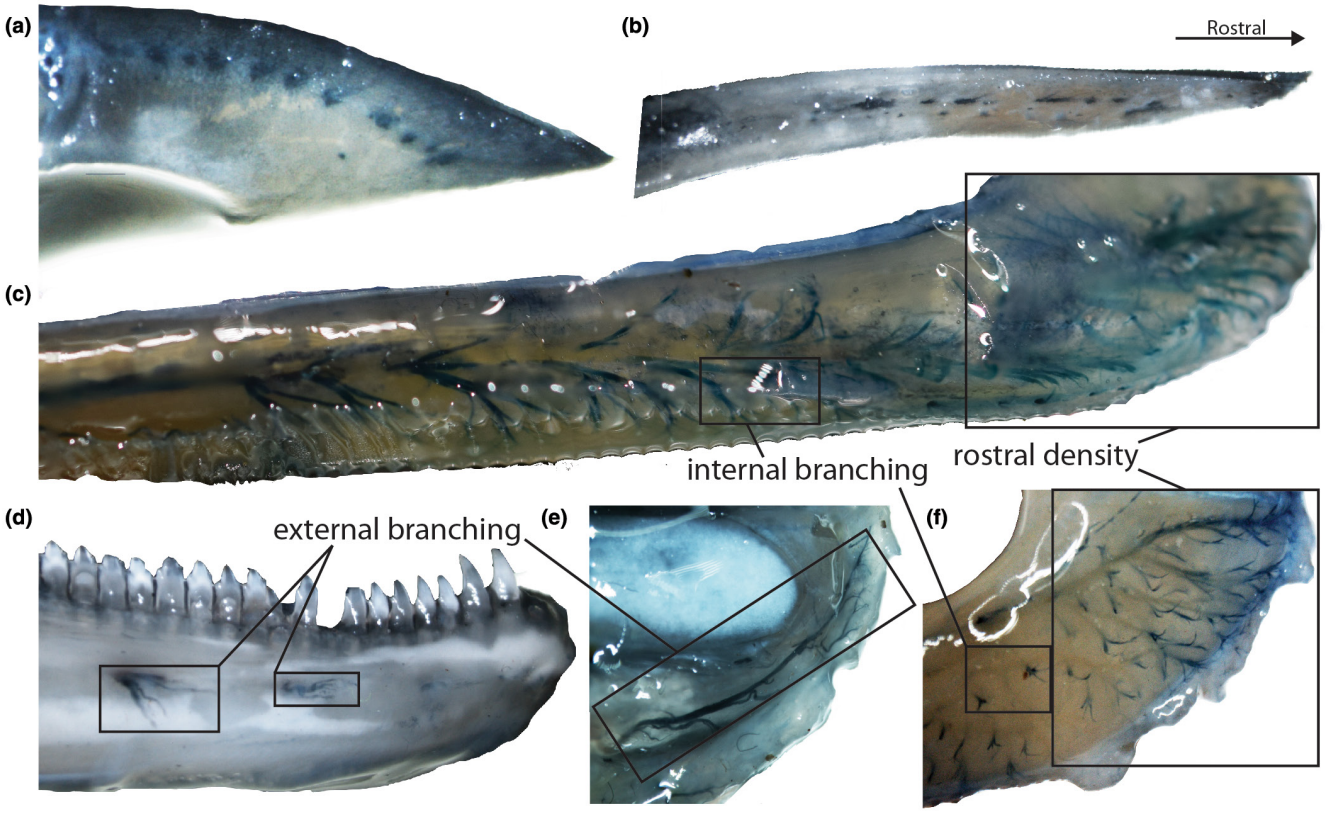

FIGURE 2 Sudan Black B staining of myelinated nerve branches in (a) *Spinus tristis* (MUVC AV287), (b) *Toxostoma rufum* (MUVC AV107), (c) *Anas platyrhynchos* (MUVC AV098), (d) *Iguana iguana* (MUVC LI036), (e) *Pantherophis* (MUVC SE002), and (f) *Alligator mississippiensis* (MUVC AL809). Hemimandibles are in left lateral view (a, d, reversed), right lateral view (b), and ventral view of the left side (c, e, f). All stained nerves are within bone with the exception of small branches in d and all branches in e.

2.5 | Derived quantities

The following quantities were calculated from combinations of the individual measurements described above:

Density metrics: Three derived quantities were used to quantify neurovascular canal distribution throughout and across the dentary. These include: dendritic density, which quantifies canal length within the dentary (total neurovascular canal length vs. dentary surface area, Figure 1a); segment frequency, which quantifies number of canal segments within the dentary (number of neurovascular canal segments vs. dentary surface area); and tip frequency, which quantifies number of tips across the dentary (number of terminal segments vs. dentary surface area) (Lessner, 2020). Residuals from these comparisons were used in the analyses described below.

Topological center of mass (topological COM): This metric quantifies the average, relative distance of terminal segments from the origin of the neurovascular canal and is collected as described by Lessner (2020). Topological orders of all segments are summed (C) and number of terminal segments tallied (n) to calculate the metric ($\bar{C}$) [$\bar{C} = C/(2n-1)$].

Topological tips: To compare branching extent along the neurovascular canal, terminal segment orders were tallied and orders scaled to canal length (in this case, the highest order per specimen; Figure 1d). This resulted in each tip being designated a percentage representing its location along the canal. To explore morphological differences across individual sections of the neurovascular canal, each canal was also divided into 10 bins and number of tips per segment tallied and compared against the total number of tips. The resulting quantities were proportions of tips per bin of the neurovascular canal. These values were used in the analyses described below.

Quantities by order: Number of Strahler segments per order were tallied per specimen to quantify overall branching patterns. The Strahler metric quantifies the overall structure of the neurovascular canal, highlighting the organization of the terminal segments (Lessner, 2020). Number of Horton first segment orders were tallied to quantify overall structure of the neurovascular canal, highlighting the organization and complexity of branches from the main canal (Lessner, 2020; Figure 1b). Relative segment lengths were collected (relative to rostrocaudal length of the dentary) and segment mean, median, and mode calculated per order to further quantify overall canal structure (Figure 1e,f).

2.6 | Analysis

The above variables were used to quantify structure of sauropsid neurovascular canals and test for shared morphological patterns

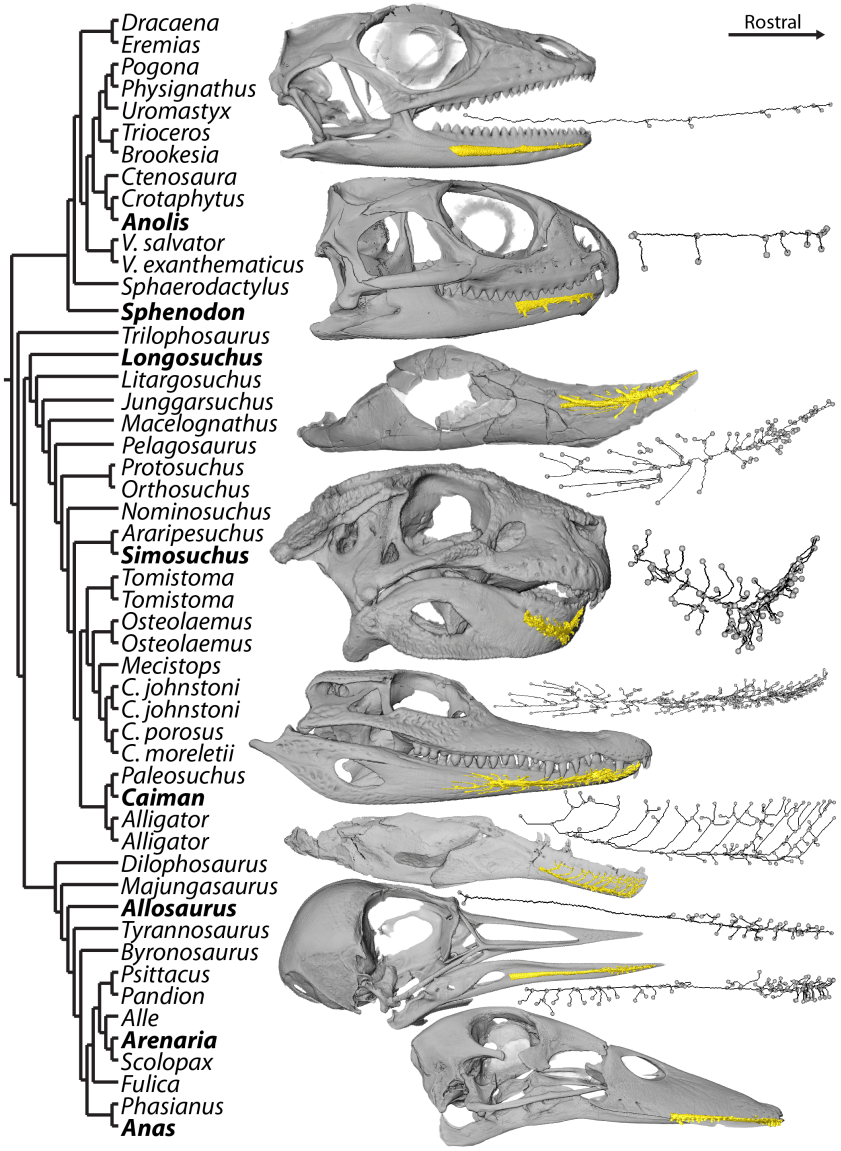

FIGURE 3 Phylogenetic representation of study taxa including 3D reconstructions of select (bolded) specimens (gray) and neurovascular canals (yellow) accompanied by simplified canal models (right)

within ecological groups. Density metric residuals were collected using phylogenetic linear models and R packages (caper) (Orme et al., 2013) and (phytools) (Revell, 2012). Based upon observed behaviors from the literature, each extant specimen was assigned to one of two groups: those highly receptive of mechanosensory cues and engaging in tactile-sensory behaviors ("tactile") and those less mechanosensitive taxa in which tactile-sensory behaviors are absent ("non-tactile") (Table 1). Group differences were confirmed for all variables in R using the (phytools) (Revell, 2012) package to run phylogenetic analyses of variance (ANOVAs). Generalized linear models (i.e., logistic regression and discriminant analysis) were used to estimate probabilities to decide group membership for fossil specimens using R packages (stats) (R Core Team, 2020), (mda) (Hastie & Tibshirani, 2020), and (arm) (Gelman & Su, 2020). The phylogeny used in analysis was an adapted phylogeny of Wilberg et al. (2019), Ruebenstahl (2019), Prum et al. (2015), and Pyron et al. (2013). Multiple specimens per species were represented as hard polytomies and branch lengths were estimated using the R package (phytools) (Revell, 2012) to calculate Pagel's lambda per variable (Pagel, 1999). Ancestral state reconstruction of binned topological tips (see below for details) was performed using the R package (ape) (Paradis & Schliep, 2019). This metric was chosen for ancestral state reconstruction because it predicts tactile ability in 10% increments, the finest discriminating model of all presented here. Branch lengths follow the phylogeny of Stockdale and Benton (2021). Taxa not included were added in Mesquite (Maddison & Maddison, 2021), and the clade Thalattosuchia was moved to reflect the location hypothesized by Wilberg et al. (2019). Variables were log-transformed (base 10) when necessary, and significance was assessed at an alpha level of $p = 0.05$.

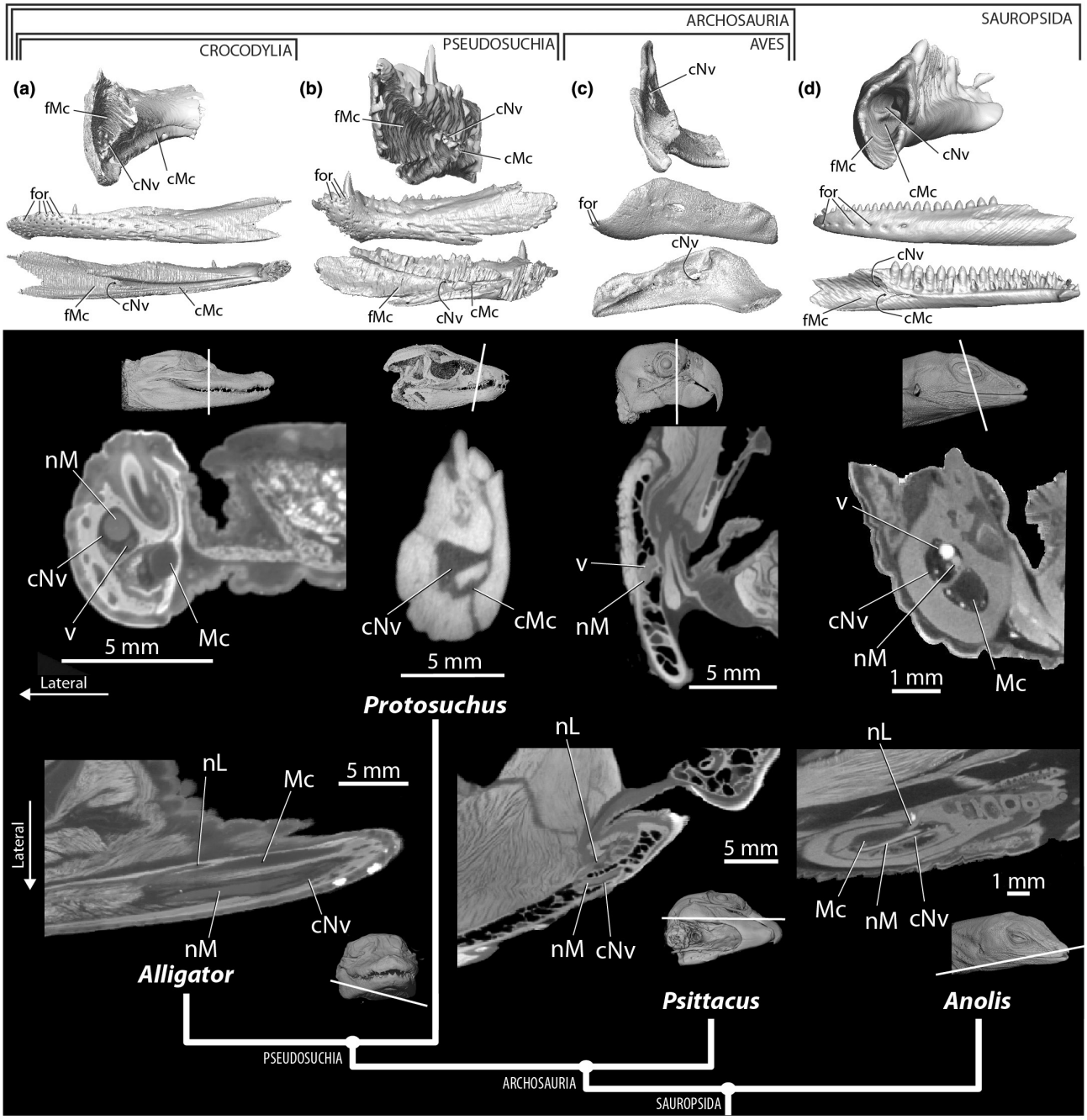

FIGURE 4 Anatomical features of the reptile mandibular canal in *Alligator* (a), the fossil pseudosuchian *Protosuchus* (b), the grey parrot *Psittacus* (c), and the anole lizard *Anolis* (d) including the bony dentary, Meckelian canal (cMc), neurovascular (cNv) canal, Meckelian fossa (fMc), and foramina (for) and the soft-tissue mandibular nerve (nM), lingual nerve (nL), vasculature (v), and Meckel's cartilage (Mc)

3 | RESULTS

3.1 | Gross anatomy

In general, the reptilian mandibular canal is a neurovascular containing canal originating from the dorsolateral aspect of the Meckelian canal in the caudal dentary (discussion of name and homology below in Discussion section), then passes rostrally, and extends branches dorsally through foramina to alveoli and rostrolaterally to the dentary integumentary surface (Figures 2 and 4). Here only branches to the integumentary surface of the dentary are quantified. Canal contents include the mandibular division of the trigeminal nerve and the mandibular artery and vein which occupy variable amounts of the canal space (Figure 4). Remarkable aspects of the mandibular canals and contents of the taxa investigated are detailed below.

The lepidosaur mandibular canal contains the small mandibular nerve dorsally and the larger mandibular artery and vein ventrally, passing through the dentary ventral to the teeth (Figure 4d). The lepidosaur mandibular canal has few accessory canals, and these begin branching from the mandibular canal just rostral to the complete

enclosure of the neurovascular canal by the dentary and separation from the Meckelian canal. This separation occurs at the level of the 23rd (from rostral) dentary tooth in *Sphaerodactylus*, the 19th tooth in *Anolis*, the 17th tooth in *Crotaphytus* and *Pogona*, the 15th tooth in *Ctenosaura*, between the 11th and 12th teeth in *Uromastyx* and *Trioceros*, the 9th tooth in *Physignathus*, the 8th tooth in *Dracaena*, and caudal to the teeth in *Varanus* and *Sphenodon*. Though rostrally, the mandibular canal becomes distinct from the lepidosaur Meckelian canal and groove, the mandibular canal remains large, dwarfing its contents in *Uromastyx*, *Trioceros*, and *Physignathus*. *Eremias*, *Crotaphytus*, *Brookesia*, and *Varanus* display a different condition in which the mandibular canal becomes distinct from Meckel's cartilage at the complete enclosure of the neurovascular canal as in crocodylians (see below; also the rostral extent of the intramandibularis muscle in *Eremias*) and the canal has little extra space around the neurovasculature. *Dracaena*, *Sphaerodactylus*, *Anolis*, *Pogona*, *Sphenodon*, and *Ctenosaura* fall in between the above conditions, with a smaller mandibular canal with some space around the contents. Sensory organs are visible to the naked eye as integumentary elevations in *Sphaerodactylus* (216) and *V. salvator* (600) and with 6 and 5 foramina, respectively, each foramen distributes to an average of 36 and 120 receptors under the assumption that nerves passing through each foramen innervate receptors equally. The foramina are arranged linearly, parallel, and ventral to the tooth row (Figure 4d).

The canal in *Trilophosaurus* follows the expected pathway from Meckelian canal to rostral dentary and has an intermediate number of terminal segments (19), when compared to the lepidosaurs (4–7) and suchians (22–194). The foramina associated with the terminal segments are arranged linearly, largely parallel to the tooth row (Figure 5a).

The avian mandibular canal takes a number of forms depending on the taxon. Generally, the canal contains the mandibular artery and vein and similarly sized mandibular nerve with little room for other tissues (Figure 4c). The mandibular nerve enters the mandible near the rostral attachment of the pseudotemporalis profundus muscle (Holliday & Witmer, 2007) first passing along the medial surface of the mandible before entering the dentary, sometimes dorsal to Meckel's cartilage (Crole & Soley, 2016). After passing through the fossa in *Struthio* and *Dromaius* Meckel's cartilage and the neurovasculature share a single canal through the mandible (Crole & Soley, 2018), and in *Phasianus* Meckel's cartilage departs the mandibular canal quite rostrally. Vessels are located either dorsal or ventral to the nerve. Because of the thin-walled dentary cortex, the distance from the canal to the keratinous beak is short and therefore branches are short. Branches typically do not occur in the caudal half of the dentary and are quite concentrated at the tip in taxa engaging in tactile-sensory behaviors (e.g., *Scolopax*, *Anas*, *Arenaria*). In some taxa (e.g., *Alle*), the canal passes through the caudal dentary before the contents exit laterally, extending forward within a deep groove on the lateral surface of the dentary before reentering the dentary at the rostral tip. In many taxa, including *Alle*, *Fulica*, *Phasianus*, and *Pandion*, the canal expands at the rostral tip of the dentary, terminating in a single, large foramen. The terminal foramina are generally clustered at the rostral tip in all avians but are not arranged in any particular pattern (Figure 4c). In *Anas* and *Scolopax*, the nerve is very large, occupying all of the mandibular canal and the canal occupying most of the dentary. In *Anas* the canal extends branches to the tomium as well as the lateral and ventral surface of the beak (these are not quantified) and terminates in an extreme density of branches at the bill tip organ (Figure 2c). This extreme density of branches is present across the rostral two-thirds of the *Scolopax* dentary and in both *Anas* and *Scolopax*, this density of nerve branches is reflected by a high density of foramina across the surface of the dentary. In *Psittacus*, additional branching of the nerve occurs in the keratin after the neurovasculature exits the rostral tip of the dentary (these branches are not included in quantitative analysis).

The crocodylian mandibular canal contains the large mandibular nerve laterally and the smaller mandibular artery and vein medially and passes through the dentary ventrolateral to the alveoli and teeth. Accessory canals begin branching from the mandibular canal to the lateral surface of the dentary at the level of the rostral termination of the intramandibularis muscle and complete enclosure of the neurovascular canal by the dentary and separation from the Meckelian canal. Small vessels accompany larger nerves laterally through these numerous canals in the dentary to ISOs (Leitch & Catania, 2012). The neurovasculature passing through an individual accessory canal supplies 2–4 sensory receptors (a range of 269–514 receptors and 85–172 foramina under the assumption that nerves passing through each foramen innervate receptors equally). Some of the foramina associated with the terminal segments are arranged in a line ventral to and paralleling the teeth, and the rest are arranged randomly, increasing in density toward the rostral tip (Figures 2f and 4a). In *A. mississippiensis*, *C. johnstoni*, *O. tetraspis*, and *P. palpebrosus* branch density notably increases near the level of the 8th and 9th dentary teeth (counted from rostral). In *T. schlegelii* a similar increase in density occurs near the level of the 15th (from rostral) dentary tooth, which seems to be a similar distance caudal from the symphysis (about 4 teeth) as the taxa listed above.

Among the extinct suchians sampled, it is only impossible to reconstruct the complete canal in *Pelagosaurus* because of poor contrast between bone and matrix. However, only the caudal origination from the mandibular canal is absent, a region lacking branches in many pseudosuchians. Otherwise, branch numbers increase rostrally in *Pelagosaurus*. The shortened and curved shape of the dentary of *Simosuchus* results in a similarly blunted mandibular canal (Figure 5s). In *Simosuchus*, the canal originates as a small invagination dorsal to the large space for Meckel's cartilage, ventrolateral to the alveoli and teeth before continuing rostrally (Figure 6i). The *Araripesuchus* mandibular canal is larger than that of *Simosuchus*, occupying more of the dentary, but smaller than that of *Nominosuchus*. Both *Araripesuchus* and *Nominosuchus* are damaged at the rostral extent, but little of the mandibular canal is missing. In *Macelognathus* the mandibular canal originates on the lateral aspect of the Meckelian canal rather than the dorsal and the canal increases in diameter in the edentulous aspect of the dentary (Figure 6d). The *Junggarsuchus* mandibular canal increases in diameter rostrally as well between the 5th and 6th teeth (from rostral) and then


(a)
(b)
(c)
(d)
(e)
(f)
(g)
(h)
(i)
(j)
(k)
(l)
(m)
(n)
(o)
(p)
(q)
(r)
(s)
(t)
(u)
(v)
(w)

FIGURE 5 Photographs of dentaries with neurovascular foramina of fossil pseudosuchians including (a) *Trilophosaurus* (TMM 31025-125), (b) Phytosaur (MNA V3601), (c) *Revueltosaurus* (PEFO 34561), (d) *Longosuchus* (TMM 31100-1338), (e) *Batrachotomus* (SMNS 80260), (f) *Hesperosuchus* (AMNH 6758), (g) *Sphenosuchus* (SAM PK-3104), (h) *Dromicosuchus* (UNC 15574), (i) *Junggarsuchus* (IVPP V14010), (j) *Macelognathus* (LACM 150148), (k) *Orthosuchus* (SAM PK-K409), (l) *Gomphosuchus* (UCMP 97638), (m) *Protosuchus* (MCZ 6727), (n) *Anatosuchus* (MNN GAD17), (o) *Hamadasuchus* (BSPG 2005 I 83), (p) *Kaprosuchus* (MNN IGU12), (q) *Araripesuchus* (BSPG 2008 I 41), (r) *Malawisuchus* (Mal-49), (s) *Simosuchus* (UA 8679), (t) *Dakosaurus* (SMNS 8203), (u) *Steneosaurus* (UC 402), (v) *Rhamphosuchus* (BMNH R5936), and (w) *Allognathosuchus* (FMNH P12141). Arrows point to select neurovascular foramina

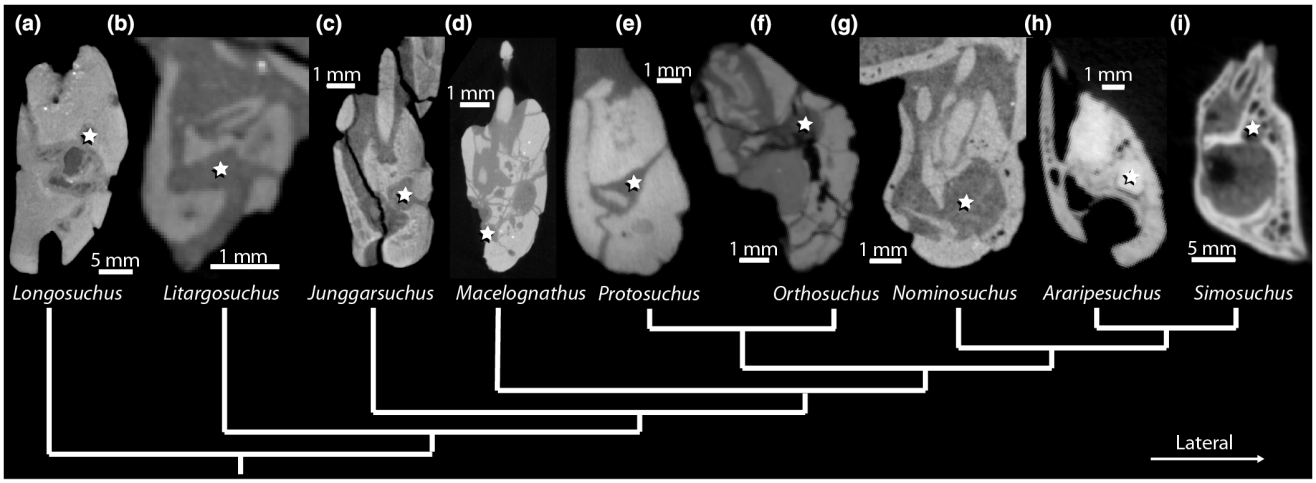

FIGURE 6 Location of mandibular canal (star) within the Meckelian fossa in non-crocodylian pseudosuchian taxa (a) *Longosuchus meadi* (TMM M-31185-84), (b) *Litargosuchus leptorhynchus* (BP-5237, reversed), (c) *Junggarsuchus sloani* (IVPP V14010), (d) *Macelognathus vagans* (LACM 150148), (e) *Protosuchus haughtoni* (BP-1-4770, reversed), (f) *Orthosuchus stormbergi* (SAM PK-K409), (g) *Nominosuchus* (IVPP 14392), (h) *Araripesuchus wegeneri* (AMNH 24450), and (i) *Simosuchus clarki* (UA 8679, reversed). Images captured in the coronal plane from CT data

quickly decreases in diameter rostrally. In *Junggarsuchus* at the level of the 8th tooth (from rostral), the Meckelian groove extends a canal laterally into the dentary, to which the mandibular canal extends a branch at the level of the 5th tooth (from rostral). Rostral to the 5th tooth in *Junggarsuchus*, this accessory Meckelian canal extends the branches to the rostromedial dentary surface, whereas the proper mandibular canal extends branches to the rostrolateral dentary surface. A similar communication between the Meckelian canal and the mandibular canal occurs between the 7th and 8th tooth from rostral in *Litargosuchus* and just caudal to the 1st tooth in *Longosuchus* (though there is an edentulous, rostral portion of the *Longosuchus* dentary). Though the dentary of *Litargosuchus* is slenderer than the other suchians investigated, the mandibular canal does not appear to decrease in diameter and therefore occupies a large cross section of the dentary. Both *Orthosuchus* and *Protosuchus* have a noticeable increase in branches at the level of the 3rd tooth (from rostral). In all taxa except for *Junggarsuchus* and *Protosuchus*, the foramina associated with the terminal segments are arranged randomly; in *Junggarsuchus* and *Protosuchus*, there is a linear arrangement ventral to the tooth row and a small rostral scattering.

3.2 | Canal contents

In lepidosaurs, nervous tissue in the caudal dentary ranges from occupying 34.3% to 5.5% of the canal, vascular tissue from 14.3% to 3%, and all other contents from 91.5% to 51.4% (Table 2; Figure 7). In the rostral lepidosaur dentary, near the symphysis, nervous tissue ranges from occupying 34.2% to 4.3%, vascular from 26.7% to 1%, and all other contents from 90.7% to 40%. In birds, nervous tissue in the caudal dentary ranges from occupying 89.8% to 7.6% of the canal, vascular tissue from 20.7% to 3%, and all other contents from 87.5% to 7.2%. In the rostral avian dentary, near the symphysis, nervous tissue ranges from occupying 68.9% to 14.8%, vascular from 40.1% to 8.5%, and all other contents from 61.8% to 22.3%. In crocodylians, nervous tissue in the caudal dentary ranges from occupying 63.5% to 26.7% of the canal, vascular tissue from 19.7% to 4.6%, and all other contents from 66.9% to 16.7%. In the rostral crocodylian dentary, near the symphysis, nervous tissue ranges from occupying 41.6% to 19.7%, vascular from 26.3% to 6.8%, and all other contents from 69.7% to 37.1%. Taxa engaging in tactile sensory behaviors have higher percentages of nervous tissue occupying canals than those that do not engage in these behaviors (Table 2).

Canal CSAs at the origin of the mandibular canal and symphyseal region are compared with skull width (a proxy for body size used for crocodyliforms by O'Brien et al., 2019). Though there is a significant, positive relationship between proximal canal CSA and skull width by pGLS ($p = 0.000$, $R^2 = 0.501$), phylogenetic ANOVA shows no significant differences between means of residuals between clades ($p = 0.952$) nor between tactile and non-tactile taxa ($p = 0.722$). There is also a significant, positive relationship

TABLE 2 Neurovascular canal contents by clade (tactile taxa shaded)

Specimen	Proximal canal CSA residual	% Nerve proximal	% Vessel proximal	% Other proximal	Symphyseal canal CSA residual	% Nerve symphysis	% Vessel symphysis	% Other symphysis
Alle alle	−0.257	23.1	17.9	59.1	−0.517	29.3	39.7	31
Anas platyrhynchos	0.988	89.8	3	7.2	0.124	61.1	11.8	27.1
Fulica americana	0.685	7.6	4.9	87.5	0.332	25.9	12.4	61.8
Pandion haliaetus	−0.995	28.1	15.3	56.6	−0.577	68.9	8.8	22.3
Phasianus colchicus	−1.337	33.8	12.7	53.5	0.133	14.8	8.5	76.7
Psittacus erithacus	−1.1545	61.5	20.7	17.9	0.172	40.3	23.5	36.3
Scolopax rusticola	0.659	63.3	13.5	23.2	0.329	36.1	40.1	23.8
Anolis sagrei	1.355	17.9	9.8	72.3	0.949	23.7	19.7	56.6
Crotaphytus collaris	−1.169	25	13	62	−0.746	22.8	22.8	54.4
Dracaena guianensis	0.349	15.5	6.2	78.3	0.138	10	7.4	82.6
Eremias arguta	0.279	15.7	3.2	81	−1.074	33.3	26.7	40
Physignathus cocincinus	−1.032	11.2	7.5	81.2	0.736	4.3	5	90.7
Pogona vitticeps	−0.883	6.2	3.1	90.8	−1.476	8.3	8.3	83.3
Sphaerodactylus caicosensis	0.124	34.3	14.3	51.4	−0.177	22.5	1	76.4
Trioceros bitaeniatus	0.424	5.5	3	91.5	0.170	14.6	10.4	75
Uromastyx geyri	−1.078	14.3	14.3	71.4	−0.785	15.7	7.8	76.5
Varanus exanthematicus	0.042	19.2	8.8	72	0.077	25.6	8.5	65.9
Varanus salvator	0.816	7.7	4.9	87.4	−1.102	34.2	22.8	43
Alligator mississippiensis	0.602	35.2	8.3	56.5	0.599	36.6	26.3	37.1
Crocodylus johnstoni	0.027	56.6	4.9	38.5	0.955	41.6	16.9	41.6
Crocodylus porosus	0.146	63.5	19.7	16.7	0.099	30.4	16.3	53.3
Osteolaemus tetraspis	−0.067	37.6	4.6	57.8	0.566	19.7	10.7	69.7
Paleosuchus palpebrosus	0.578	26.7	6.4	66.9	0.282	34.7	17.5	47.8
Tomistoma schlegelii	0.901	33.3	5.3	61.5	0.793	36.4	6.8	56.8
Araripesuchus wegeneri	−0.212	–	–	–	0.745	–	–	–
Junggarsuchus sloani	−0.316	–	–	–	0.054	–	–	–
Litargosuchus leptorhynchus	−1.192	–	–	–	−0.435	–	–	–
Nominosuchus	1.101	–	–	–	0.888	–	–	–
Orthosuchus stormbergi	−1.152	–	–	–	−0.157	–	–	–
Protosuchus haughtoni	−3.039	–	–	–	−0.181	–	–	–
Simosuchus clarki	−0.580	–	–	–	1.133	–	–	–

between symphyseal canal CSA and skull width by phylogenetic generalized least squares regression (pGLS) ($p = 0.000$, $R^2 = 0.844$), and phylogenetic ANOVA of means of residuals between clades shows no significant differences between clades ($p = 0.856$) nor between tactile and non-tactile taxa ($p = 0.595$). Though relationships are insignificant, it does appear that taxa engaging in tactile sensory behaviors exhibit larger CSAs (Figure 7). Pearson correlations coefficients between canal and nerve contents are 0.565 for the proximal canal ($p = 0.004$) and 0.922 for the symphyseal canal ($p < 0.001$). Correlations coefficients between canal and vessel contents are 0.819 for the proximal canal ($p < 0.001$) and 0.726 for the symphyseal canal ($p < 0.001$).

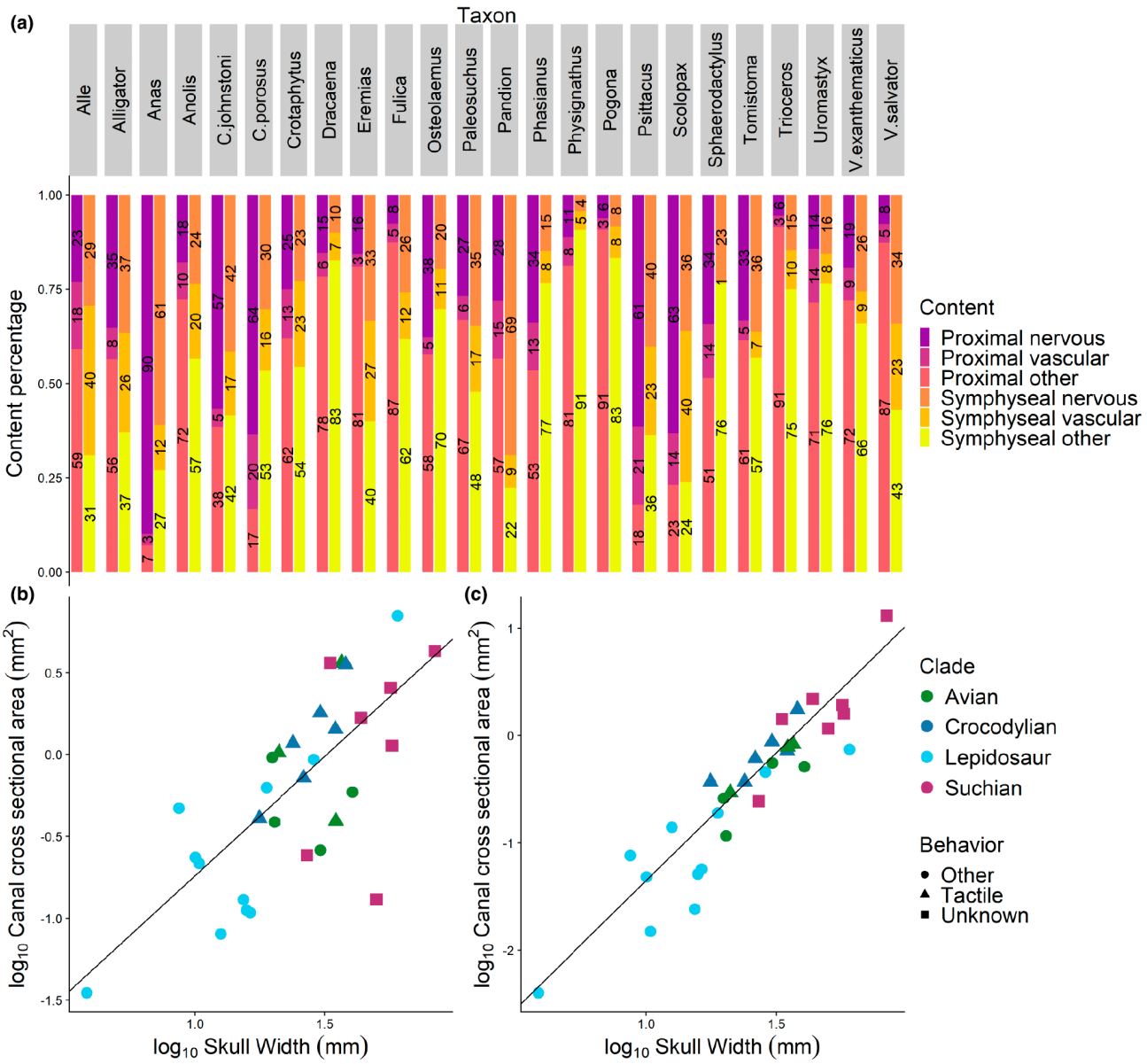

FIGURE 7 Proximal and symphyseal canal contents of extant taxa by percentage (a), and cross-sectional area of mandibular canal at the proximal end (b) and symphysis (c) versus skull width by clade and ecology of extant and select extinct (see Table S1) taxa

3.3 | Topological tips

Crocodylians show a high density of tips along entire length of the canal with an increase in density at the rostral end of the dentary (Figure 8c; Figure S1). Lepidosaurs have few tips, but these are evenly spaced across the canal. *Trilophosaurus* shares a similar pattern. Some birds follow a similar pattern as lepidosaurs, but birds with tactile ecologies (e.g., *Anas*, *Scolopax*) have higher densities of tips across the length of the canal and highest tip densities at the rostral end of the dentary. Fossil suchians show similar tip distributions to avians. Within extinct pseudosuchians, the dentary has tips spread uniformly across the dentary with most taxa (except for *Longosuchus*, *Nominosuchus*, and *Araripesuchus*) also exhibiting an increase in tips at the rostral end.

Topological tips are binned (10 bins of equal length per specimen) to determine how terminal segments are distributed across the dentary (Figure S1). Phylogenetic ANOVA of numbers of tips per bin (Figure S1) shows no significant difference in tips across the length by clade ($p = 0.319$). However, tactile and non-tactile taxa do have near-significant differences in tip distribution across the length of the canal ($p = 0.043$).

Binned tips are compared using linear discriminate analysis among the extant taxa. The resulting model predicts extant ecology with 91% accuracy (only *Arenaria* and *Psittacus* with nearly incorrect predictions), with few posterior probabilities within 20% of one another. The resulting model is used to predict ecology in the fossil taxa and bin predictions of all taxa are compiled into a "percent tactile" (Figure 9; Table 1) (empty bins are scored as 0% tactile on the basis that tactile sensation requires innervation). The fossil posterior probabilities are also largely not within a 20% margin. Excluding just *C. johnstoni* (TMM M-6807) at 70%,

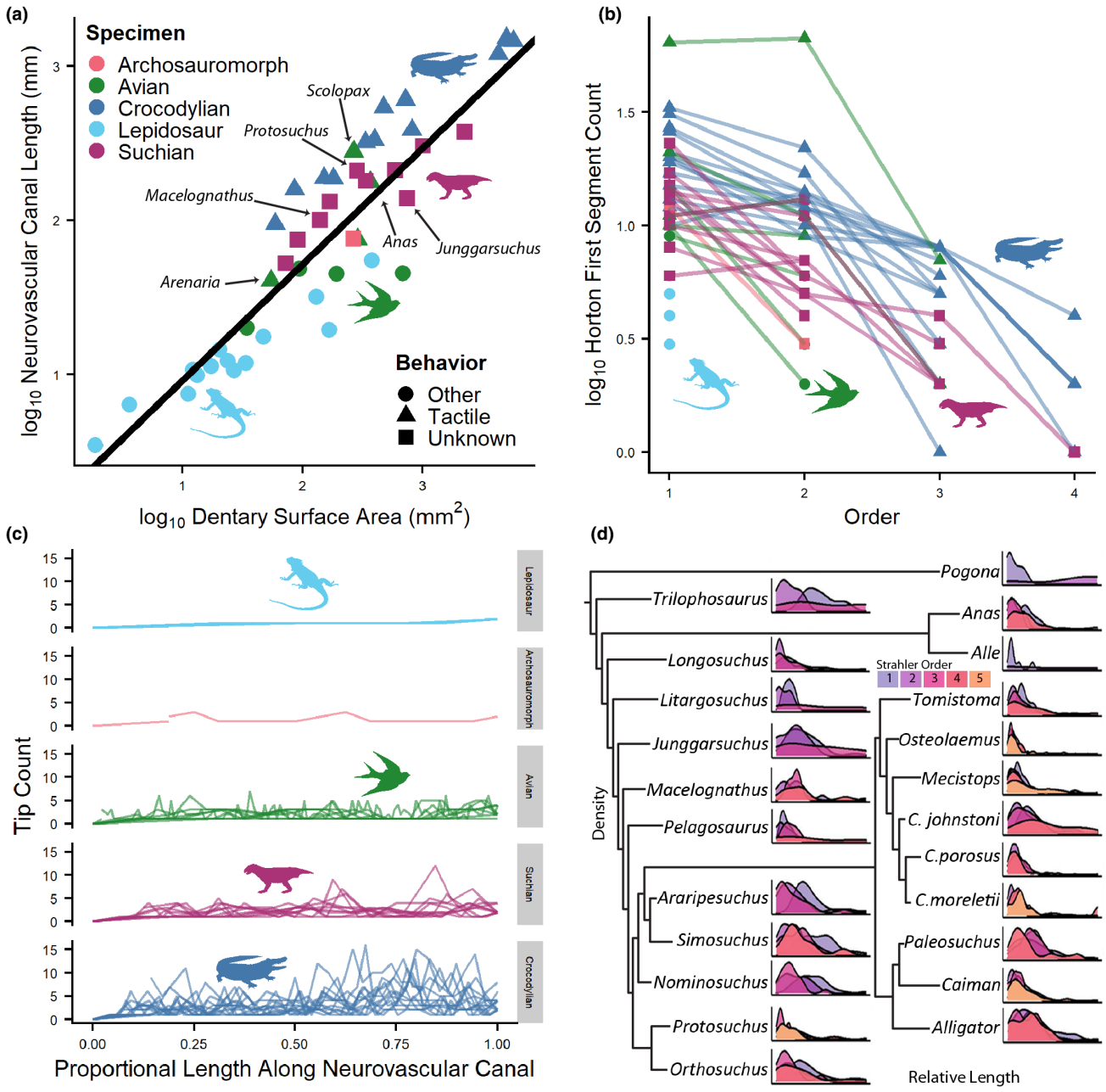

FIGURE 8 Comparative branching quantifications including dendritic density (a), branch complexity (b), branch distribution (c), and segment structure (d)

all crocodylian taxa are 80%–100% tactile. Tactile avian taxa are between 50% and 100% tactile and non-tactile avian taxa between 10% and 60% tactile. Lepidosaurs are between 0% and 10% tactile. All suchians are between 20% and 80% tactile, and *Trilophosaurus* is 20% tactile.

3.4 | Density metrics and topological COM

Dendritic density: By pGLS, there is a significant, positive relationship between rostral dentary surface area and total canal length ($p = 0.000$, $R^2 = 0.8471$) among all taxa (Figure 8a; Figure S2). Residuals of this relationship are collected to represent a single metric for dendritic density. In extant taxa, clade means are not significantly different ($p = 0.332$) but differences between tactile and non-tactile taxa are nearly significant ($p = 0.063$) as revealed by phylogenetic ANOVA.

Segment frequency: By pGLS, there is a significant, positive relationship between rostral dentary surface area and number of canal segments ($p = 0.0000$) (Figure S2). However, there is some variability in the data ($R^2 = 0.5296$). Residuals of this relationship are collected to represent a single metric for segment frequency. In extant taxa, clade means are not significantly different ($p = 0.274$), but differences between tactile and non-tactile taxa are significant ($p = 0.019$) as revealed by phylogenetic ANOVA.

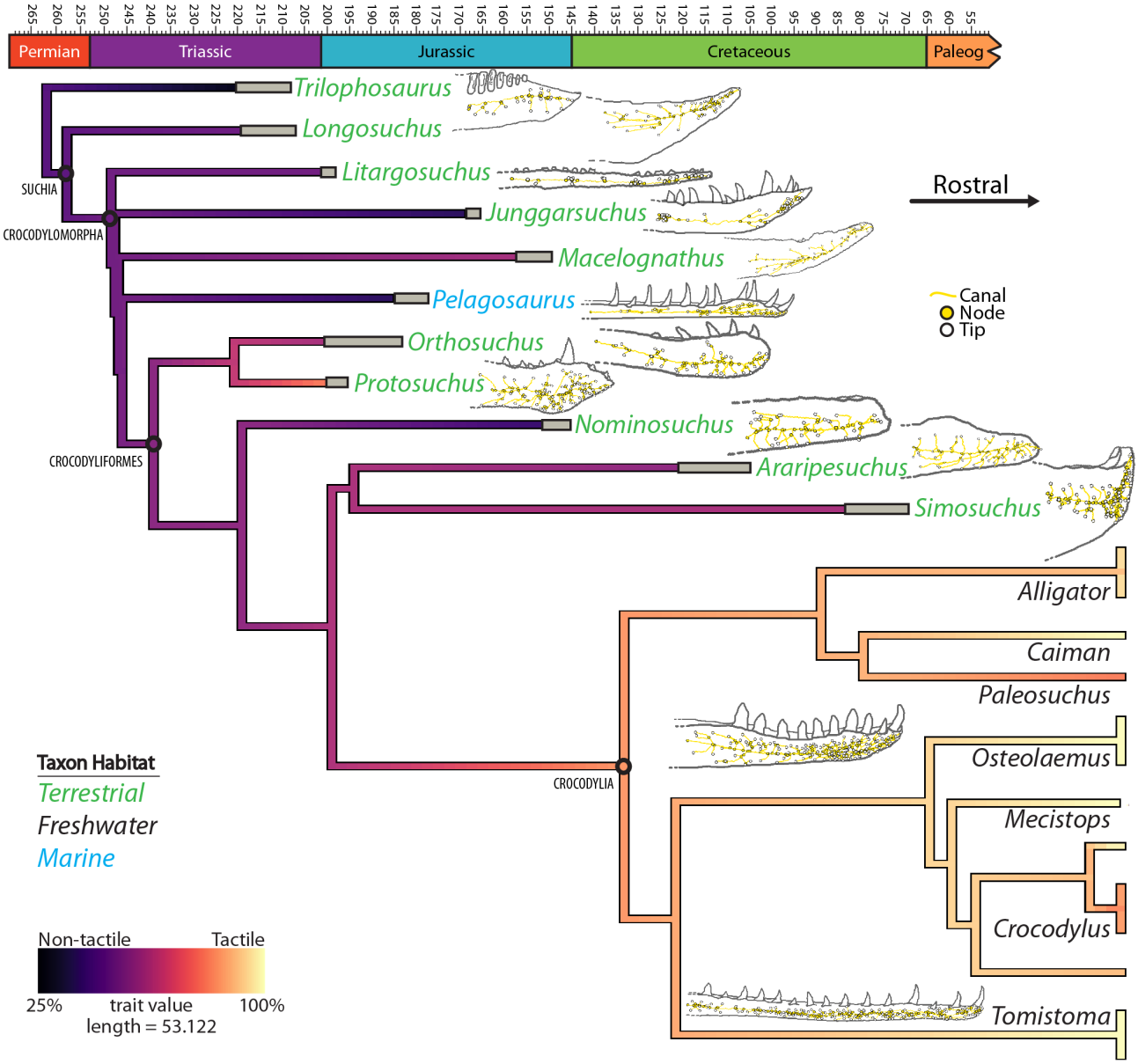

FIGURE 9 Evolution of pseudosuchian trigeminal sensory abilities showing statistically hypothesized ancestral state reconstruction of a stepwise increase in enhanced tactile sensation. Phylogeny colors represent percent tactile, calculated from binned topological tips. Taxa colors represent habitat

Tip frequency: By pGLS, there is a significant, positive relationship between rostral dentary surface area and number of terminal segments ($p = 0.000$) (Figure S2). However, there is some variability in the data ($R^2 = 0.476$). Residuals of this relationship are collected to represent a single metric for tip frequency. In extant taxa, clade means are not significantly different ($p = 0.445$), but differences between tactile and non-tactile taxa are nearly significant ($p = 0.073$) as revealed by phylogenetic ANOVA.

Topological COM: By pGLS, there is a significant, positive relationship between rostral dentary surface area and topological COM ($p = 0.0000$) (Figure S2). However, there is some variability in the data ($R^2 = 0.5427$). Residuals of this relationship are collected to represent a single metric for topological COM. In extant taxa, clade means are not significantly different ($p = 0.472$), but differences between tactile and non-tactile taxa are nearly significant ($p = 0.100$) as revealed by phylogenetic ANOVA.

Residuals of the above density metrics and topological COM against rostral dentary surface area are collected to represent single values for the metrics and compared using linear discriminant analysis of the extant taxa. The resulting model predicts extant ecology with 97% accuracy (only *Fulica* being predicted incorrectly), with few posterior probabilities within 70% of one another. The resulting model is used to predict ecology in the fossil taxa (Table 1). The fossil posterior probabilities are also largely not within a 30% margin.

3.5 | Quantities by order

Strahler segment counts: Crocodylians and *Scolopax* have the most segments and lepidosaurs the fewest, with all other avian and fossil taxa falling in between (Figure S3). Two patterns are evident. The first, seen in lepidosaurs, some avians, and some fossil taxa, segment count decreases as order decreases. The second forms a "check-mark," seen in crocodylians, some avians, and some fossil taxa, where count order decreases to the second to last order present and then increases to the final order. In extant taxa, phylogenetic ANOVA shows clade means are significantly different ($p = 0.001$), with significant differences between avians, lepidosaurs, and crocodylians. Differences between tactile and non-tactile taxa are significant ($p = 0.001$).

Segment counts per order are compared with extant ecology with multiple regression and only first-order segment counts are found to be significant ($p = 0.02835$). Logistic regression using only extant, first-order segment counts predicts extant ecology with 97% accuracy (only *Arenaria* being predicted incorrectly) and with a 60% margin between posterior probabilities. Probabilities from prediction of fossil ecology by first-order segment counts (Table 1) are not within a 20% margin.

Horton first segment counts: Among most taxa (all but *Scolopax*, *Mecistops*, and *Araripesuchus*), there are fewer first segments as order increases (Figure 8b; Figure S3). Crocodylians and *Protosuchus* have first segments up to Horton order 4, whereas lepidosaurs only have first segments of Horton order 1. All other taxa fall in between. Phylogenetic ANOVA of extant taxa shows clade means are nearly significantly different ($p = 0.074$), but differences between tactile and non-tactile taxa are significant ($p = 0.015$).

Horton first segment counts per order are compared with extant ecology with multiple regression and only first- and second-order first segment counts are found to be significant ($p = 0.00585$, $p = 0.00302$). Logistic regression using only extant, first- and second-order first segment counts predicts extant ecology with 95% accuracy (only *Arenaria* and *Phasianus* are predicted incorrectly and only for first-order first segments) with a 20% margin between posterior probabilities. Probabilities from prediction of fossil ecology by first and second first segment counts (Table 1) are not within an 18% margin.

Mean relative segment lengths: Exploring mean segment lengths per Strahler order relative to rostrocaudal dentary length (Lessner, 2020), lepidosaur segments are the longest and crocodylian and *Scolopax* segments the shortest, with all other taxa falling between (Figure S4). In lepidosaurs and *Alle*, second-order relative segment means are higher than first order, whereas second-order relative segment means are lower that first order in other taxa. Phylogenetic ANOVA of extant taxa shows clade means are significantly different ($p = 0.003$), with a significant difference between lepidosaurs and crocodylians and a nearly significant difference between lepidosaurs and avians. Differences between tactile and non-tactile taxa are significant ($p = 0.001$).

Mean segment lengths per order are compared with extant ecology with multiple regression and only first-, second-, and third-order segments are found to be significant ($p = 0.0258$, $p = 0.0294$, $p = 0.0301$). Logistic regression using only extant, first-, second-, and third-order segment means predicts extant ecology with 98% accuracy (only *Arenaria* and *Phasianus* predicted incorrectly for order 3) with a 20% margin between most posterior probabilities. Probabilities from predictions of fossil ecology by first, second, and third relative mean segment lengths are mostly not within a 25% margin and predictions are reported as a percentage (Table 1).

Median relative segment lengths: Exploring median segment lengths per Strahler order relative to total canal length (Lessner, 2020), results follow that described for mean relative segment lengths above with clade means significantly differing ($p = 0.027$) and pairwise corrected *p*-values indicating near significant differences between crocodylians and lepidosaurs and avians and lepidosaurs. Ecological means differ significantly ($p = 0.001$) (Figure S4). As above, first-, second-, and third-order segments are found to be significant with multiple regression ($p = 0.0001$, $p = 0.00008$, $p = 0.00008$), and logistic regression using extant first, second, and third segment medians predicts extant ecology with 91% accuracy (only *Paleosuchus*, *Pandion*, and *Psittacus* are predicted incorrectly for second-order segments and *Fulica*, *Sphaerodactylus*, and *Trioceros* for first) with a 20% margin between most posterior probabilities. Probabilities from predictions of fossil ecology by first, second, and third relative median segment lengths are mostly not within a 20% margin, and predictions are reported as a percentage (Table 1).

Mode relative segment lengths: Exploring mode segment lengths per Strahler order relative to rostrocaudal dentary lengths (Lessner, 2020), lepidosaur segments are longest and crocodylians shortest with all other taxa falling between (Figure 8d; Figure S4). For all lepidosaurian taxa, most second-order segments are longer than first-order segments, though for all other taxa, this is the opposite. Phylogenetic ANOVA of extant taxa shows clade means are significantly different ($p = 0.006$) but pairwise corrected p-values show significant differences between lepidosaurs and crocodylians only. Differences between tactile and non-tactile taxa are significant ($p = 0.004$). As above, first-, second-, and third-order segments are found to be significant with multiple regression ($p = 0.00006$, $p = 0.001$, $p = 0.001$), and logistic regression using extant first, second, and third segment modes predicts extant ecology with 93% accuracy (only *Anas*, *C. johnstoni* [TMM M-6807], *Fulica*, and *Paleosuchus* first order and *Pandion* second and third orders are predicted incorrectly), with few posterior probabilities within a 40% margin. Probabilities from predictions of fossil ecology by first, second, and third relative mode segment lengths are mostly not within a 20% margin, and predictions are reported as a percentage (Table 1).

4 | DISCUSSION

4.1 | Assumptions, limitations, and constraints

In nature, there are rarely absolutes. Here for ease of prediction, we categorized taxa as "tactile" and "non-tactile" based on behaviors documented by the literature (Table 1). Some models (e.g., density metrics

and topological COM, Strahler segments, and Horton first segments) predict sensitivity in a binary manner, whereas the other models (e.g., topological tips, segment lengths) predict a range of sensitivities. Ideally, physiological testing among reptiles would provide measurable values of tactile sensitivity that would strengthen the form-function relationship used in the predictive model for extinct taxa. However, such neuroethological work is beyond the scope of this paper.

As usual, unbalanced sampling affects interpretation of results. In choosing extant specimens, organisms were selected from across the clade and ecologies. Fossil specimens were limited to availability and completeness. The absence of crocodylomorphs informative to terrestrial–semiaquatic transitions, including thalattosuchians, tethysuchians, and early neosuchians, is noted and due to several factors: (1) complete rostral dentaries were required for this project, and mandibles are not always preserved or collected, (2) for adequate CT reconstruction, specimens had to be robust enough to handle, largely undistorted, and free of density artifacts, and (3) though some colleagues shared CT data, others did not, therefore limiting available data.

Before exploring the predictions derived from the metrics and models described below, we consider several assumptions. These predictions are based on an osteological correlate (i.e., the mandibular canal) of a soft tissue feature (i.e., mandibular nerve). This study quantifies the bony morphology necessary to distribute nerves and enable trigeminal-innervated tactile sensation in extant taxa and assesses the same bony morphology in extinct taxa. In most extant taxa, neurovascular canal contents were verified (Figure 4; Table 1) and nerves are present. However, canal contents are quite variable (Figure 7), and therefore remain uncertain in extinct taxa and predictions tentative. Though regardless of canal contents, among the extant taxa explored, dendritic branching only occurs in taxa exhibiting tactile sensory. Additionally, among reptiles not all nerve distribution and branching occur within bone (Figure 2). It is possible that additional branching once nerves enter integument allows for widespread distribution of nervous tissue. Along the same lines, for this project we must overlook potential physiological differences related to speed of signal transmission, central nervous system processing, and neuronal density.

Because dentary length was used as a size proxy in metrics relying on size (i.e., mean, median, and mode relative neurovascular canal segment lengths), predictions based on these metrics may not be completely accurate in the cases of taxa with longirostrine versus brevirostrine dentaries (e.g., *Litargosuchus* vs. *Simosuchus*). Also, exploring segment lengths relative to total canal length reveals any comparative patterns among taxa are overwhelmed by and simply reflect the number of segments present (Lessner, 2020). It is expected this method would work for fragmentary specimens as well even though an incomplete dentary means an incomplete neurovascular canal; comparisons likely hold true regardless of the presence of the caudal end of the dentary. Dentary length was used as a size proxy in the absence of complete skulls for all taxa, in which case skull width might be a useful replacement for body size (O'Brien et al., 2019). Skull width was tested for mean segment lengths, but differences are not significant between ecologies ($p = 0.509$). However, predictions of tactile ability decreased in many extant taxa and increased in many lepidosaurs and extinct taxa (Table 1).

Predictions based on Strahler segment counts are only made using first order (i.e., terminal) neurovascular canal segments. It is expected that there is a minimum number of terminal segments per surface area necessary for even non-tactile taxa to innervate integument at minimal sensitivity. Larger non-tactile organisms likely require more terminal segments to similarly innervate integument than smaller ones do. However, nerve distribution and size also appear to be limited in larger organisms, constraining sensory abilities (More et al., 2010). Large body size poses an issue in that the time a nerve takes to conduct a signal along the length of its axons to the central nervous system (responsiveness) is dependent on axon diameter. More et al. (2010) demonstrated that it was not possible for an elephant to increase nerve CSA to maintain the signal speed and/or receptive field size (resolution) present in a shrew. Though axon numbers and diameters do increase, responsiveness and resolutions are still lower. As such, signal delays are up to 17 times longer in large mammals than small mammals (More & Donelan, 2018). However, Manor et al. (1991) show signal speed is slowed by branching in axons, and therefore larger animals may be able to maintain comparative signal speeds by having fewer terminal receptors; though receptive fields would shrink as a result.

These findings suggest an increase in terminal segments (i.e., foramina) is not enough to distribute the neurovasculature for tactile-sensory morphology. Foramina in the dentary mark the location of the terminal nerve segments within the bone. Terminal canal segment (i.e., foramina) distribution was quantified in the past in the context of reptilian extra-oral tissues (e.g., gums, lips, teeth, Morhardt, 2009), which receive innervation from the trigeminal nerve. Meanwhile, simple, qualitative observations on the presence of foramina are instead cited as evidence for crocodylian level sensitivity in fossil reptiles (Álvarez–Herrera et al., 2020; Barker et al., 2017; Carr et al., 2017; Cau et al., 2017; Cerroni et al., 2020; Ibrahim et al., 2014; Martill et al., 2021; Rothschild & Naples, 2017). In addition to increasing tips, the branching itself must complexify and tip density must increase. This is reflected in the trend from a non-tactile rating in all lepidosaurian taxa, to neutral in *Trilophosaurus* and some pseudosuchians, to tactile in more derived pseudosuchian taxa (Table 1) and the data for tip frequency (Figure S1). It is also reflected in qualitative observation of foramina across the dentaries of numerous archosaurian taxa (Figure 5). Therefore, the use of surface foramina alone as proxies for trigeminal-innervated sensation lack veracity.

4.2 | Ecomorphological metrics

Overall, the results show statistically supported, quantitative morphological differences between extant taxa that are highly receptive of mechanosensory cues and engage in tactile sensory behaviors (deemed "tactile") and less mechanosensitive taxa in which tactile-sensory behaviors are absent (deemed "non-tactile"). In contrast with the tactile crocodylians and tactile-foraging birds examined, non-tactile

lepidosaurs and birds have lower densities, fewer total segments, and more-simply branched distributions of neurovascular canals (detailed specifically in the paragraphs below). The differences are both observable on the gross morphological level and statistically significant. Though lepidosaurs and crocodylians possess independently distinct morphologies, the avian species span the gap, exhibiting a diversity of morphologies consistent with their diverse range of ecologies.

Similarities in neurovascular tip distribution are present among crocodylians and birds with bill tip organs indicating a unique morphology is necessary for a specialized sensory ecology. The topological ordering method reveal high counts of tips across the dentary (independent of size) in extant taxa engaging in tactile sensory behaviors in contrast to few tips across the dentary in non-tactile taxa. In addition, extant tactile taxa have a higher density of tips at the rostral end of the mandible (Figures 2 and 8c). This finding corroborates the presence of bill tip organs in ducks and probing birds (Avilova, 2018; Berkhoudt, 1976; Cunningham et al., 2013; Hoerschelmann, 1972). Thus, this finding also supports the hypothesis that the rostral end of crocodylian mandibles functions akin to a bill tip organ, possessing nerve tips with smaller receptive fields and increased discriminatory abilities in comparison with the rest of the mandible (Leitch & Catania, 2012). The basal archosaurian condition is a mandibular canal with few, evenly distributed tips along the dentary as found in the lepidosaurian taxa and the archosauriform *Trilophosaurus* (Figures 8c; Figure S1). The increase in number of tips rostrally on the mandible among extinct pseudosuchians suggests origins of the derived, extant crocodylian condition within earlier-diverging crocodyliforms. Terminal segment distribution may be visualized by observation of foramina on the dentary surface (Figure 5). Among reptiles there tends to be a line of terminal segments just ventral to and paralleling the alveoli. In archosaurs, another line of terminal segments parallels the ventral border of the dentary. Among basal pseudosuchians, there are few randomly distributed foramina across the rostralmost dentary whereas among neosuchians, there are far more foramina distributed densely across much of the dentary (Figure 5).

Tactile taxa have more densely innervated faces than non-tactile taxa again supporting that a specific morphology is required for enhanced tactile sensory abilities. Density metrics (i.e., residuals of dendritic density, segment frequency, tip frequency) are all larger in taxa engaging in tactile sensory behaviors than non-tactile taxa. Large density metrics indicate increased distribution of nervous tissue to integument covering the dentary and therefore increased discrimination and decreased receptive field size (Figure 8a; Figure S2). Similarly, the large topological COM in taxa engaging in tactile-sensory behavior indicates a larger distance (in segments) between the origin of the canal to terminal segments. As such, a larger topological COM suggests more accessory branching and topological complexity regardless of size within the dentaries of taxa engaging in tactile sensory behaviors. The predictive model developed from this set of values was the most accurate (at 97%). The categorization of *Fulica* as tactile rather than the non-tactile status it was assigned may signal morphological and sensory convergence with ducks. In fact, feeding convergence is present among coots, dabbling ducks, and other waterfowl (Allouche & Tamisier, 1984), and similar feeding styles may necessitate similar sensory requirements.

Segment arrangements are similar among tactile taxa, which possess higher numbers of more complex neurovascular canal segments, differing from the relatively simple morphology present in non-tactile taxa. Strahler segment counts are in agreement with topological COM values. Larger Strahler segment counts are present in taxa engaging in tactile sensory behaviors and smaller counts are present in non-tactile taxa (Figure S3). Additionally, in non-tactile taxa, segment count tends to decrease as order increases, which is the case for tactile taxa until the final order, in which there is an increase in segment counts. The highest ordered segments in the Strahler ordering method are the segments along the caudal portion of the main canal. More of these segments means that complicated branches (i.e., with third or fourth order first segments) are present immediately at the rostral end of the canal. Fewer high-order segments means that such complicated branches are absent, or they occur further caudally. Exploration of Horton branches confirms this (Figure 8b). Non-tactile taxa have few Horton branches larger than Horton-order two. Branches in the mandibles of tactile taxa are more complex than those in non-tactile taxa, and there are also more branches, thus distributing a higher density of tips across the density.

The three metrics used to quantify relative Strahler neurovascular segment length (i.e., mean, median, and mode) generally provide the same results (Figure 8d; Figures S4 and S5). Segment length results again indicate *Fulica*'s categorization as non-tactile may be incorrect (see above). The longer length of lepidosaur segments relative to tactile taxa seems to be because the lack of branches fail to break the neurovascular canal into segments. Longer second-order segments in lepidosaurs than in other taxa reflect the lack of interruption of second-order segments by additional branches. This trend continues in other taxa in which higher-order segments tend to be longest because their terminal nature means they are uninterrupted. When taxa have high segment counts, frequency of short segments is often higher (Figure 8d; Figures S4 and S5).

4.3 | The mandibular canal, morphology, and homology

The diversity and homology of the canal passing through the dentary (i.e., mandibular canal, inferior alveolar canal) among reptiles has received little attention in the literature and is here termed the "mandibular canal" to include edentulous taxa. The origin of the reptilian mandibular canal is the "Meckelian canal," within the Meckelian fossa (Romer, 1956), but neurovasculature and Meckel's cartilage do not share the same spaces in all taxa.

Among non-avian reptiles, Meckel's cartilage and the mandibular neurovasculature typically pass through the Meckelian fossa together but are enclosed by distinct canals further rostrally (Oelrich, 1956). This division occurs just rostral to the medially branching oral intermandibular nerve (lingual nerve, mylohyoid nerve; Abdel-Kader

et al., 2011; Oelrich, 1956; Poglayen-Neuwall, 1953; Watkinson, 1906) and is often obscured medially by the splenial in intact mandibles (Figure 4). This division also marks the caudal extent of accessory canals and is near the rostral extent of the intramandibularis muscle in crocodylians, lacertid lepidosaurs (e.g., *Eremias*), and charadriiform (e.g., *Alle*) and procellariform birds.

Most birds too possess a "Meckelian fossa" (*fossa aditus canalis mandibulae*; Baumel & Witmer, 1993), but Meckel's cartilage is not present in all adult birds. In developing birds and those in which the cartilage persists (e.g., ostrich, emu), the cartilage is present ventral to the nerve caudally and medial to the nerve rostrally (Crole & Soley, 2018). In birds both with and lacking Meckel's cartilage, there is a single mandibular canal. The mandibular canals of extinct species of non-avian and avian dinosaurs are rarely described. A foramen within the Meckelian canal is noted in the archosauriform *Osmolskina* and hypothesized to house the mandibular nerve (Borsuk–Białynicka & Evans, 2009). A neurovascular foramen is also described within the Meckelian canal in a putative hylaeochampsid eusuchian (Yi et al., 2016). With respect to theropod dinosaurs, the Meckelian groove in *Poekilopleuron*, *Allosaurus*, and *Sinraptor* contains dorsal and ventral foramina, and the dorsal canal is hypothesized to have housed the mandibular neurovasculature (Allain, 2002). In the context of edentulism, Wang et al. (2017) detail an additional alveolar canal dorsal to the mandibular canal in *Limusaurus*, Caenagnathidae, and *Sapeornis* that is likely homologous to the alveoli of toothed archosaurs.

Comparative CT data allow for clarification, helping distinguish canals, distribution, and contents (in the case of contrast-enhanced data, Figure 4). A canal may be identified as transmitting the mandibular neurovasculature if it communicates with alveoli or the tomial surface as well as the lateral integumentary surface. Among the reptiles investigated in this study, the percentage of canal contents vary both rostrocaudally within an individual and among individuals (Figure 7). The only evident trend is that the taxa engaging in tactile sensory behaviors dedicate more canal space to nervous tissue than taxa not engaging in tactile sensory behaviors. Exploring the CSA of the mandibular canal as an osteological correlate for nervous or vascular contents reveals that the proximal CSA is not well correlated with nervous CSA and is somewhat correlated with vascular CSA. The canal at the symphysis is well correlated with nerve CSA and somewhat correlated with vascular CSA. However, since there is no significant relationship between mandibular canal CSA and ecology in extant taxa, in combination with the observation that canal contents are highly variable, mandibular canal CSA cannot be used to predict sensory ability in fossil taxa. Similarly, volume of the mandibular canal is not a reliable proxy for sensory ability, especially because of the varied overlap with Meckel's cartilage and distribution to differing numbers of teeth.

4.4 | Paleoecological implications in pseudosuchian transitions

Pseudosuchia proves to be a useful group to evaluate hypotheses of changing trigeminal tissues with shifting ecologies. Osteological correlates of nerves in pseudosuchians are robust and habitat shifts are well known. Early-diverging pseudosuchians occupied terrestrial habitats from their origins in the Early Triassic (+245 Ma) (Figure 9; Nesbitt, 2011). Two habitat shifts by non-surviving clades include the transition from a terrestrial to marine habitat by thalattosuchians tentatively in the Early Jurassic (~195 Ma) and a transition from a terrestrial to freshwater habitats by some notosuchian crocodyliforms in the Early Cretaceous (~130 Ma) (Wilberg et al., 2019). Along the neosuchian line to modern crocodylians, a transition from terrestrial to freshwater and marine habitats occurred in the Middle Jurassic (~174.1 Ma) (Figure 9; Wilberg et al., 2019). These ecological shifts are tied with morphological shifts (e.g., inner ear, Brusatte et al., 2016; Schwab et al., 2020, and body size, Gearty & Payne, 2020) and our data demonstrate that these were accompanied by changes in sensory systems toward the extant condition as well.

Overall, whereas phylogeny was not found to significantly influence morphological diversity of extant species, morphology was found to differ among tactile and non-tactile taxa. Models predicted extant tactile ecology with 91%–98% accuracy and thus are used to predict somatosensory ecology in fossil taxa (Table 1). The predictive models verified pseudosuchians and their relatives possessed the necessary bony morphology to facilitate a range of trigeminal-innervated tactile sensory abilities and stepwise acquisition of extreme trigeminal sensation along the line to crocodyliforms (Figure 9). Results from this study (i.e., low segment/branch counts, small topological COM, low density metrics, few topological tips) suggest the primitive archosaurian condition was one lacking the necessary morphology for enhanced tactile sensation. This is indicated by the lepidosaurian morphology as well as that of the terrestrial archosauromorph *Trilophosaurus*. Ancestral state reconstruction at the base of Archosauria (47% tactile) reveals an increase in tactile sensory ability from the primitive condition (0%–20% in non-archosaurs), though not one substantial enough to allow for the enhanced tactile sensation of extant crocodylians (87%; Figure 9). Quantification of the neurovascular canals of early-diverging, terrestrial pseudosuchian *Longosuchus* confirms an intermediate morphology (i.e., intermediate segment/branch counts, density metrics, topological tips) and predicts a sensory ability between non-tactile taxa and crocodylians. At the base of Crocodylomorpha, ancestral state reconstruction predicts little increase in sensory ability past that present at the base of Archosauria (50%). The intermediate morphology is present in the terrestrial crocodylomorphs *Litargosuchus* and *Macelognathus*, though sensory abilities are predicted to be nearing the lower range of extant crocodylians in *Macelognathus*. Among the non-crocodyliform crocodylomorphs examined, only *Junggarsuchus* exhibits a morphology of less tactile potential than predicted to be present at the base of Crocodylomorpha. In Crocodyliformes, ancestral state reconstruction predicts higher potential for tactile sensory ability (55%) than at the base of Crocodylomorpha. This is not reflected in the early-diverging, marine crocodyliform *Pelagosaurus* which demonstrates a morphology and tactile prediction similar to *Junggarsuchus*. However, within Crocodyliformes, terrestrial protosuchids *Protosuchus* and *Orthosuchus* are quantified with similar potential for tactile sensory abilities as *Macelognathus*.

Though the later-diverging terrestrial crocodyliform *Nominosuchus* demonstrates a less-tactile morphology, similar to *Litargosuchus* and *Longosuchus*, later diverging, terrestrial notosuchians *Araripesuchus* and *Simosuchus* are comparable to the protosuchids in morphology and predicted sensory ability. Though *Macelognathus*, *Protosuchus*, *Orthosuchus*, *Araripesuchus*, and *Simosuchus* approach the lower range of extant crocodylian sensation, ancestral state reconstruction still predicts a 26% increase in tactile sensory abilities from Neosuchia (61%) to Crocodylia (87%).

These morphologies indicate specialized tactile sensory abilities in most early terrestrial crocodylomorphs by the Jurassic (Figure 9). Therefore, an increase in tactile sensation appeared before the mesoeucrocodylian radiation and before neosuchians entered aquatic habitats in the Middle-Late Jurassic (Wilberg et al., 2019). Divergence dates for the first taxa rated as having the morphology for tactile sensory ecologies (i.e., *Macelognathus* and the protosuchids) are in the Late Triassic (Leardi et al., 2017; Turner et al., 2017) meaning the tactile-sensing morphology was present within pseudosuchians by this point. The increase in trigeminal sensory abilities suggested by this data indicates the sensory transition preceded the terrestrial to semiaquatic transition in the Middle Jurassic (Wilberg et al., 2019). The lack of ecological data surrounding use of the trigeminal sensory system as a specialized tool by extant terrestrial reptiles and even broader limits hypotheses of function in extinct pseudosuchians. Evidence is limited to probe-foraging birds, and star-nosed moles, which are highly derived and exhibit morphologies with unique functions (Catania, 2011; Cunningham et al., 2013). In any case, the rostral location of the increase in canal density and complexity indicates the mandibles were more capable of receiving stimuli during substrate contact behaviors such as grubbing or burrowing though additional morphological and taphonomic evidence are necessary to confirm such behaviors.

Our timeline conflicts with the previously hypothesized Early Jurassic origin of crocodylian-like facial sensation (Soares, 2002), and our conclusions from quantitative approaches differ from earlier qualitative interpretations of *Protosuchus* and other terrestrial crocodylomorphs. Other aspects of the trigeminal system are useful in sensory ability prediction but are not used to conclude the timing of origins of the extant crocodylian condition (George & Holliday, 2013). Secondary reductions in the trigeminal sensory system are also proposed for marine taxa as a result of tradeoffs with other sensory systems (e.g., tethysuchian *Rhabdognathus*, thalattosuchians; George & Holliday, 2013; Bowman et al., 2021). Our data for the marine thalattosuchian *Pelagosaurus* also suggest minimal trigeminal sensory abilities, which may be convergent or a characteristic of the clade depending on the phylogenetic position of thalattosuchians (Ruebenstahl, 2019; Wilberg, 2015).

5 | CONCLUSIONS

Here we quantify structural differences among mandibular canals of reptilian taxa and demonstrate variation is consistent with sensory ecologies. We contrast the morphological complexity (e.g., highly branched, densely packed canals) required for taxa (e.g., crocodylians, probe-foraging birds) engaging in tactile sensory behaviors with the lack of complexity present in taxa (e.g., other birds, lepidosaurs) not engaging in such behaviors providing a basis for predictions of behavior and feeding ecology in extinct organisms. Enhanced facial sensation remains a key innovation in living crocodylians and was also likely critical for the successful occupation of semiaquatic habitats by Jurassic pseudosuchians. The indication that the pseudosuchian tactile trigeminal morphology preceded their terrestrial–semiaquatic transition is yet another example of sensory innovations preceding species diversification (Carlson & Arnegard, 2011; Parker, 2011). Exploring similar trigeminal sensory transitions in other clades (e.g., evolution of whiskers in mammals, bill tip organs in birds) may reveal morphological and ecological trends. These methods may also be useful in fragmentary materials where only portions of the dentary are available as demonstrated by the presence of significant differences between ecological groups across regions of the dentary (Figure S1). Isolation of dentary regions may also lead to easier detection of regions of increased sensitivity (i.e., bill tip organs). Finally, combination of branching analysis with other trigeminal-related metrics (e.g., trigeminal ganglion volume) and their associated osteological correlates (e.g., trigeminal foramen diameter) will strengthen ecomorphological groups and hypotheses of sensory abilities in extinct animals.

AUTHOR CONTRIBUTIONS

Emily J. Lessner provided funding and data, synthesized the project, collected and analyzed data, created figures, and wrote the manuscript. Kathleen N. Dollman provided data and edited the manuscript. James M. Clark provided data and edited the manuscript. Xing Xu provided data and edited the manuscript. Casey M. Holliday helped conceive the project, provided funding and data, and edited the manuscript.

ACKNOWLEDGMENTS

We thank Kevin Middleton for comments and him and Austin Lawrence for advice on statistical analysis. Thanks to Tara Selley, Jim Schiffbauer, and MizzoμX; and Jessie Maisano, Matt Colbert, and UTCT for CT scanning. Thanks to University of Texas Vertebrate Collections and Matt Brown, Chris Sagebiel, and Kenny Bader; the Florida Keys Wild Bird Rehabilitation Center; Ruth Elsey and the Rockefeller State Refuge; the FMNH and Alan Resetar, and Bruce Young for specimen access. Additional thanks to Morphosource, Digimorph (NSF grant IIS-9874781), Jonah Choiniere, Nate Kley, Alan Turner, Pat O'Connor, and Marc Jones, and for data sharing and transfer.

FUNDING INFORMATION

This work was supported by the National Science Foundation Division of Earth Sciences (NSF EAR 1631684, 1762458, 1636753) and Division of Integrative Organismal Biology (NSF IOS 1457319); Missouri Research Board; Evolving Earth Foundation; Society of Vertebrate Paleontology; University of Missouri Life Sciences

Fellowship Program; Department of Pathology and Anatomical Sciences, University of Missouri School of Medicine; National Science Foundation of China (42288201, 41688103).

DATA AVAILABILITY STATEMENT

Data and code used in analysis are available at https://osf.io/kt6y3/ and Table S1 provides CT scan availability information per specimen.

INSTITUTIONAL ABBREVIATIONS

AMNH, American Museum of Natural History, New York, New York, USA; BMNH, Natural History Museum, London, England; BP, Bernard Price Institute for Paleontological Research, Johannesburg, South Africa; BRSLI, Bath Royal Literary and Scientific Institution, Bath, England; BSPG, Bayerische Staatssammlung für Paläenotologie und Geologie, Munich, Germany; FMNH, Field Museum of Natural History, Chicago, Illinois, USA; IVPP, Institute of Vertebrate Paleontology and Paleoanthropology, Beijing, China; LACM, Natural History Museum of Los Angeles County, Los Angeles, California, USA; MAL, Malawi Department of Antiquities, Malawi; MCZ, Museum of Comparative Zoology, Cambridge, Massachusetts, USA; MNA, Museum of Northern Arizona, Flagstaff, Arizona, USA; MNN, Musée National du Niger, Niamey, République due Niger; MUVC, University of Missouri Vertebrate Collection, Columbia, Missouri, USA; OUVC, Ohio University Vertebrate Collection, Athens, Ohio, USA; PEFO, Petrified Forest National Park, Arizona, USA; SAM, South African Museum, Cape Town, Western Cape Province, South Africa; SAMA, South Australia Museum, Adelaide, Australia; SMNS, State Museum of Natural History, Stuttgart, Germany; TMM, Texas Memorial Museum, Austin, Texas, USA; UA, Université d'Antananarivo, Antananarivo, Madagascar; UADBA, Université d'Antananarivo, Département de Biologie Animale, Antananarivo, Madagascar; UC, University of Chicago, Chicago, Illinois, USA; UCMP, University of California Museum of Paleontology, Berkeley, California, USA; UF, University of Florida, Gainesville, Florida, USA; UNC, University of North Carolina, Chapel Hill, North Carolina, USA; USNM, Smithsonian National Museum of Natural History, Washington, D.C., USA.

ORCID

Emily J. Lessner https://orcid.org/0000-0003-0774-1613
Kathleen N. Dollman https://orcid.org/0000-0002-5468-4896
James M. Clark https://orcid.org/0000-0003-0980-4315
Xing Xu https://orcid.org/0000-0002-4786-9948
Casey M. Holliday https://orcid.org/0000-0001-8210-8434

REFERENCES

Abdel-Kader, T.G., Ali, R.S. & Ibrahim, N.M. (2011) The cranial nerves of *Mabuya quinquetaeniata* III: nervus trigeminus. *Life Science Journal*, 8, 650–669.

Allain, R. (2002) Discovery of megalosaur (Dinosauria, Theropoda) in the Middle Bathonian of Normandy (France) and its implications for the phylogeny of basal Tetanurae. *Journal of Vertebrate Paleontology*, 22(3), 548–563.

Alonso, P.D., Milner, A.C., Ketcham, R.A., Cookson, M.J. & Rowe, T.B. (2004) The avian nature of the brain and inner ear of *Archaeopteryx*. *Nature*, 430(7000), 666–669.

Allouche, L. & Tamisier, A. (1984) Feeding convergence of gadwall, coot and the other herbivorous waterfowl species wintering in the Camargue: a preliminary approach. *Wild*, 35, 135–142.

Álvarez-Herrera, G., Agnolin, F. & Novas, F. (2020) A rostral neurovascular system in the mosasaur *Taniwhasaurus antarcticus*. *The Science of Nature*, 107(3), 1–5.

Ananjeva, N.B., Dilmuchamedov, M.E. & Matveyeva, T.N. (1991) The skin sense organs of some iguanian lizards. *Journal of Herpetology*, 25(2), 186–199.

Angielczyk, K.D. & Schmitz, L. (2014) Nocturnality in synapsids predates the origin of mammals by over 100 million years. *Proceedings of the Royal Society B: Biological Sciences*, 281(1793), 20141642.

Avilova, K.V. (2018) Spatial organization of the epithelial structures in the bill tip organ of waterfowl (Anseriformes, Aves). *Zhurnal Obschei Biologii*, 78(1), 25–37.

Barbas-Henry, H.A. & Lohman, A.H. (1986) The motor complex and primary projections of the trigeminal nerve in the monitor lizard, *Varanus exanthematicus*. *Journal of Comparative Neurology*, 254(3), 314–329.

Barker, C.T., Naish, D., Newham, E., Katsamenis, O.L. & Dyke, G. (2017) Complex neuroanatomy in the rostrum of the Isle of Wight theropod *Neovenator salerii*. *Scientific Reports*, 7(1), 1–8.

Baumel, J.J. & Witmer, L.M. (1993) Osteologia. In: Baumel, J.J. (Ed.) *Handbook of avian anatomy: Nomina anatomica avium*, 2nd edition. Cambridge, MA: Publications of the Nuttall Ornithological Club, pp. 45–132.

Berkhoudt, H. (1972) The epidermal structure of the bill tip organ in ducks. *Netherlands Journal of Zoology*, 26(4), 561–566.

Berkhoudt, H. (1976) The epidermal structure of the bill tip organ in ducks. *Netherlands Journal of Zoology*, 26(4), 561–566.

Berkhoudt, H. (1980) The morphology and distribution of cutaneous mechanoreceptors (Herbst and Grandry corpuscles) in bill and tongue of the mallard (*Anas platyrhynchos l.*). *Netherlands Journal of Zoology*, 30, 1–34.

Borsuk–Białynicka, M. & Evans, S.E. (2009) Cranial and mandibular osteology of the early Triassic archosauriform *Osmolskina czatkowicensis* from Poland. *Palaeontologia Polonica*, 65, 235–281.

Bowman, C.I., Young, M.T., Schwab, J.A., Walsh, S., Witmer, L.M., Herrera, Y. et al. (2021) Rostral neurovasculature indicates sensory trade-offs in Mesozoic pelagic crocodylomorphs. *The Anatomical Record*, 305(10), 2654–2669.

Breyer, H. (1929) Uber Hautsinnesorgane und Hautung bei der Lacertilien. *Zoologische Jarbücher (Anatomie)*, 51, 549–581.

Bronzati, M., Benson, R.B., Evers, S.W., Ezcurra, M.D., Cabreira, S.F., Choiniere, J. et al. (2021) Deep evolutionary diversification of semicircular canals in archosaurs. *Current Biology*, 31(12), 2520–2529.

Brusatte, S.L., Benton, M.J., Lloyd, G.T., Ruta, M. & Wang, S.C. (2010) Macroevolutionary patterns in the evolutionary radiation of archosaurs (Tetrapoda: Diapsida). *Earth and Environmental Science Transactions of the Royal Society of Edinburgh*, 101(3–4), 367–382.

Brusatte, S.L., Muir, A., Young, M.T., Walsh, S., Steel, L. & Witmer, L.M. (2016) The braincase and neurosensory anatomy of an early Jurassic marine crocodylomorph: implications for crocodylian sinus evolution and sensory transitions. *The Anatomical Record*, 299(11), 1511–1530.

Carlson, B.A. & Arnegard, M.E. (2011) Neural innovations and the diversification of African weakly electric fishes. *Communicative & Integrative Biology*, 4(6), 720–725.

Carr, T.D., Varricchio, D.J., Sedlmayr, J.C., Roberts, E.M. & Moore, J.R. (2017) A new tyrannosaur with evidence for anagenesis and crocodile-like facial sensory system. *Scientific Reports*, 7(1), 1–11.

Catania, K.C. (2011) The sense of touch in the star-nosed mole: from mechanoreceptors to the brain. *Philosophical Transactions of the Royal Society B: Biological Sciences*, 366(1581), 3016–3025.

Cau, A., Beyrand, V., Voeten, D.F., Fernandez, V., Tafforeau, P., Stein, K. et al. (2017) Synchrotron scanning reveals amphibious ecomorphology in a new clade of bird-like dinosaurs. *Nature*, 552(7685), 395–399.

Cerroni, M.A., Canale, J.I., Novas, F.E. & Paulina-Carabajal, A. (2020) An exceptional neurovascular system in abelisaurid theropod skull: new evidence from *Skorpiovenator bustingorryi*. *Journal of Anatomy*, 240, 612–626.

Cooper, W.E., Jr. (1994) Prey chemical discrimination, foraging mode, and phylogeny. In: Vitt, L.J. & Pianka, E.R. (Eds.) *Lizard ecology: historical and experimental perspectives*. Princeton, NJ: Princeton University Press, pp. 95–116.

Crole, M.R. & Soley, J.T. (2014) Comparative distribution and arrangement of Herbst corpuscles in the oropharynx of the ostrich (*Struthio camelus*) and emu (*Dromaius novaehollandiae*). *The Anatomical Record*, 297(7), 1338–1348.

Crole, M.R. & Soley, J.T. (2016) Comparative morphology, morphometry and distribution pattern of the trigeminal nerve branches supplying the bill tip in the ostrich (*Struthio camelus*) and emu (*Dromaius novaehollandiae*). *Acta Zoologica*, 97, 49–59.

Crole, M.R. & Soley, J.T. (2018) Persistence of Meckel's cartilage in subadult *Struthio camelus* and *Dromaius novaehollandiae*. *Acta Zoologica*, 101, 97–205.

Cunningham, S.J., Alley, M.R., Castro, I., Potter, M.A., Cunningham, M. & Pyne, M.J. (2010) Bill morphology of ibises suggests a remote-tactile sensory system for prey detection. *The Auk*, 127(2), 308–316.

Cunningham, S.J., Corfield, J.R., Iwaniuk, A.N., Castro, I., Alley, M.R., Birkhead, T.R. et al. (2013) The anatomy of the bill tip of kiwi and associated somatosensory regions of the brain: comparisons with shorebirds. *PLoS One*, 8(11), e80036.

Di-Poï, N. & Milinkovitch, M.C. (2013) Crocodylians evolved scattered multi-sensory micro-organs. *EvoDevo*, 4(1), 1–19.

du Toit, C.J., Chinsamy, A. & Cunningham, S.J. (2022) Comparative morphology and soft tissue histology of the remote-touch bill-tip organ in three ibis species of differing foraging ecology. *Journal of Anatomy*, 241, 966–980.

Filipski, G.T. & Wilson, M.V.H. (1986) Nerve staining using Sudan Black B and its potential use in comparative anatomy. In: Wadding, J. & Rudkin, D.M. (Eds.) *Proceedings of the 1985 workshop on care and maintenance of natural history collections*. Toronto: Royal Ontario Museum Life Sciences Miscellaneous Publication, pp. 33–36.

Gans, C. (1975) Tetrapod limblessness: evolution and functional corollaries. *American Zoologist*, 15(2), 455–467.

Gans, C. & Northcutt, R.G. (1983) Neural crest and the origin of vertebrates: a new head. *Science*, 220(4594), 268–273.

Gearty, W. & Payne, J.L. (2020) Physiological constraints on body size distributions in Crocodyliformes. *Evolution*, 74(2), 245–255.

Gelman, A. & Su, Y. (2020) arm: data analysis using regression and multilevel/hierarchical models. R package version 1.11-2. from: https://CRAN.R-project.org/package=arm [Accessed 15 September 2020].

George, I.D. & Holliday, C.M. (2013) Trigeminal nerve morphology in *Alligator mississippiensis* and its significance for crocodyliform facial sensation and evolution. *The Anatomical Record*, 296(4), 670–680

Gignac, P.M., Kley, N.J., Clarke, J.A., Colbert, M.W., Morhardt, A.C., Cerio, D. et al. (2016) Diffusible iodine-based contrast-enhanced computed tomography (diceCT): an emerging tool for rapid, high-resolution, 3-D imaging of metazoan soft tissues. *Journal of Anatomy*, 228(6), 889–909.

Grace, M.S., Church, D.R., Kelly, C.T., Lynn, W.F. & Cooper, T.M. (1999) The Python pit organ: imaging and immunocytochemical analysis of an extremely sensitive natural infrared detector. *Biosensors and Bioelectronics*, 14(1), 53–59.

Grap, N.J., Machts, T., Essert, S. & Bleckmann, H. (2020) Stimulus discrimination and surface wave source localization in crocodilians. *Zoology*, 139, 125743.

Gutiérrez-Ibáñez, C., Iwaniuk, A.N. & Wylie, D.R. (2009) The independent evolution of the enlargement of the principal sensory nucleus of the trigeminal nerve in three different groups of birds. *Brain, Behavior and Evolution*, 74(4), 280–294.

Hastie, T. & Tibshirani, R. (2020) mda: mixture and flexible discriminant analysis. R package version 0.5.2. from: http://CRAN.R-project.org/package=mda [Accessed 15 September 2020].

Hiller, U. (1968) Untersuchungen zum Feinbau und zur Funktion der Haftborsten von Rep- tilien. *Zeitschrift für Morphologie und Ökologie der Tiere*, 62, 307–362.

Hiller, U. (1978) Morphology and electrophysiological properties of cutaneous sensilla in agamid lizards. *Pflügers archiv*, 377(2), 189–191.

Hoerschelmann, H. (1972) Strukturen der Schnabelkammer bei Schnepfenvölgen (Charadriidae und Scolopacidae). *Zeitscrift für wissenschaftliche Zoologie Journal*, 185, 105–121.

Holliday, C.M. & Witmer, L.M. (2007) Archosaur adductor chamber evolution: integration of musculoskeletal and topological criteria in jaw muscle homology. *Journal of Morphology*, 268, 457–484.

Holliday, C.M. & Witmer, L.M. (2009) The epipterygoid of crocodyliforms and its significance for the evolution of the orbitotemporal region of eusuchians. *Journal of Vertebrate Paleontology*, 29(3), 715–733.

Hopson, J.A. (1979) Paleoneurology. *Biology of the Reptilia*, 9(2), 39–148.

Ibrahim, N., Sereno, P.C., Dal Sasso, C., Maganuco, S., Fabbri, M., Martill, D.M. et al. (2014) Semiaquatic adaptations in a giant predatory dinosaur. *Science*, 345(6204), 1613–1616.

Jackson, M.K. & Doetsch, G.S. (1977) Response properties of mechanosensitive nerve fibers innervating cephalic skin of the Texas rat snake. *Experimental Neurology*, 56(1), 78–90.

Landmann, L. (1975) The sense organs in the skin of the head of Squamata (Reptilia). *Israel Journal of Ecology and Evolution*, 24(3-4), 99–135.

Leardi, J.M., Pol, D. & Clark, J.M. (2017) Detailed anatomy of the braincase of *Macelognathus vagans* marsh, 1884 (Archosauria, Crocodylomorpha) using high resolution tomography and new insights on basal crocodylomorph phylogeny. *PeerJ*, 5, e2801.

Leitch, D.B. & Catania, K.C. (2012) Structure, innervation and response properties of integumentary sensory organs in crocodilians. *Journal of Experimental Biology*, 215(23), 4217–4230.

Lessner, E.J. (2020) Quantifying neurovascular canal branching patterns reveals a shared crocodylian arrangement. *Journal of Morphology*, 282(2), 185–204.

Lessner, E.J., Elsey, R.M. & Holliday, C.M. (2022) Ontogeny of the trigeminal system and associated structures in *Alligator mississippiensis*. *Journal of Morphology*, 283, 1210–1230.

MacIver, M.A., Schmitz, L., Mugan, U., Murphey, T.D. & Mobley, C.D. (2017) Massive increase in visual range preceded the origin of terrestrial vertebrates. *Proceedings of the National Academy of Sciences of the United States of America*, 114(12), E2375–E2384.

Maddison, W. P. & Maddison, D.R. (2021) Mesquite: a modular system for evolutionary analysis. Version 3.70. Available from: http://www.mesquiteproject.org [Accessed 15th September 2020].

Manor, Y., Koch, C. & Segev, I. (1991) Effect of geometrical irregularities on propagation delay in axonal trees. *Biophysical Journal*, 60(6), 1424–1437.

Martill, D.M., Smith, R.E., Longrich, N. & Brown, J. (2021) Evidence for tactile foraging in pterosaurs: a sensitive tip to the beak of *Lonchodraco giganteus* (Pterosauria, Lonchodectidae) from the Upper Cretaceous of southern England. *Cretaceous Research*, 117, 104637.

Martin, G.R. (2007) Visual fields and their functions in birds. *Journal of Ornithology*, 148(2), 547–562.

Martin, G.R. (2012) Through birds' eyes: insights into avian sensory ecology. *Journal of Ornithology*, 153(Supplement 1), 23–48.

Martin, G.R. & Coetzee, H.C. (2004) Visual fields in hornbills: precision-grasping and sunshades. *Ibis*, 146(1), 18–26.

Matveyeva, T.N. & Ananjeva, N.B. (1995) The distribution and number of the skin sense organs of agamid, iguanid and gekkonid lizards. *Journal of Zoology*, 235(2), 253–268.

More, H.L. & Donelan, J.M. (2018) Scaling of sensorimotor delays in terrestrial mammals. *Proceedings of the Royal Society B*, 285(1885), 20180613.

More, H.L., Hutchinson, J.R., Collins, D.F., Weber, D.J., Aung, S.K. & Donelan, J.M. (2010) Scaling of sensorimotor control in terrestrial mammals. *Proceedings of the Royal Society B: Biological Sciences*, 277(1700), 3563–3568.

Morhardt, A.C. (2009) Dinosaur smiles: do the texture and morphology of the premaxilla, maxilla, and dentary bones of sauropsids provide osteological correlates for inferring extra-oral structures reliably in dinosaurs? Master thesis, Western Illinois University.

Neenan, J.M., Reich, T., Evers, S.W., Druckenmiller, P.S., Voeten, D.F., Choiniere, J.N. et al. (2017) Evolution of the sauropterygian labyrinth with increasingly pelagic lifestyles. *Current Biology*, 27(24), 3852–3858.

Nesbitt, S.J. (2011) The early evolution of archosaurs: relationships and the origin of major clades. *Bulletin of the American Museum of Natural History*, 352, 1–292.

O'Brien, H.D., Lynch, L.M., Vliet, K.A., Brueggen, J., Erickson, G.M. & Gignac, P.M. (2019) Crocodylian head width allometry and phylogenetic prediction of body size in extinct crocodyliforms. *Integrative Organismal Biology*, 1(1), obz006.

Oelrich, T.M. (1956) *The anatomy of the head of Ctenosaura pectinata (Iguanidae)*. Ann Arbor, MI: University of Michigan Museum of Zoology Miscellaneous Publications.

Orejas-Miranda, B., Zug, G.R., Garcia, D.Y. & Achaval, F. (1977) Scale organs of the head of Leptotyphlops (Reptilia, Serpentes), a variational study. *Proceedings of the Biological Society of Washington*, 90, 209–213.

Orme, D., Freckleton, R., Thomas, G., Petzoldt, T., Fritz, S., Isaac, N. et al. (2013) caper: comparative analysis of phylogenetics and evolution in R. R package version 0.5.2. from: http://CRAN.Rproject.org/package=caper [Accessed 15 September 2020].

Pagel, M. (1999) Inferring the historical patterns of biological evolution. *Nature*, 401(6756), 877–884.

Paradis, E. & Schliep, K. (2019) ape 5.0: an environment for modern phylogenetics and evolutionary analyses in R. *Bioinformatics*, 35, 526–528.

Parker, A.R. (2011) On the origin of optics. *Optics & Laser Technology*, 43(2), 323–329.

Poglayen-Neuwall, I. (1953) Studies of jaw muscles and of their innervation in crocodiles. *Anatomischer Anzeiger*, 99(16–17), 257–276.

Prum, R.O., Berv, J.S., Dornburg, A., Field, D.J., Townsend, J.P., Lemmon, E.M. et al. (2015) A comprehensive phylogeny of birds (Aves) using targeted next-generation DNA sequencing. *Nature*, 526(7574), 569–573.

Pyron, R.A., Burbrink, F.T. & Wiens, J.J. (2013) A phylogeny and revised classification of Squamata, including 4161 species of lizards and snakes. *BMC Evolutionary Biology*, 13(1), 1–54.

R Core Team. (2020) *R: a language and environment for statistical computing*. Vienna, Austria. R Foundation for Statistical Computing. from: https://www.R-project.org/ [Accessed 15 September 2020].

Revell, L.J. (2012) phytools: an R package for phylogenetic comparative biology (and other things). *Methods in Ecology & Evolution*, 3, 217–223. Available from: https://doi.org/10.1111/j.2041-210X.2011.00169.x

Romer, A.S. (1956) *Osteology of the reptiles*. Chicago: University of Chicago Press.

Rothschild, B.M. & Naples, V. (2017) Apparent sixth sense in theropod evolution: the making of a cretaceous weathervane. *PLoS One*, 12(11), e0187064.

Ruebenstahl, A.A. (2019) Junggarsuchus sloani, an early late Jurassic crocodylomorph with crocodyliform affinities. Master's thesis, The George Washington University.

Ryan, M.J. (1990) Sexual selection, sensory systems and sensory exploitation. *Oxford Surveys in Evolutionary Biology*, 7, 157–195.

Schmidt, W. (1920) Einiges fiber die Hautsinnesorgane der Agamiden insbesonders von Calotes, nebst Be- merkungen iiber diese Organe bei Gekkonidae und Iguanidae. *Anatomischer Anzeiger*, 53, 11.

Schmitz, L. & Motani, R. (2011) Nocturnality in dinosaurs inferred from scleral ring and orbit morphology. *Science*, 332(6030), 705–708.

Schneider, C.A., Rasband, W.S. & Eliceiri, K.W. (2012) NIH image to ImageJ: 25 years of image analysis. *Nature Methods*, 9(7), 671–675.

Schwab, J.A., Young, M.T., Neenan, J.M., Walsh, S.A., Witmer, L.M., Herrera, Y. et al. (2020) Inner ear sensory system changes as extinct crocodylomorphs transitioned from land to water. *Proceedings of the National Academy of Sciences of the United States of America*, 117(19), 10422–10428.

Schwenk, K. (1994) Comparative biology and the importance of cladistic classification: a case study from the sensory biology of squamate reptiles. *Biological Journal of the Linnean Society*, 52(1), 69–82.

Sherbrooke, W.C. & Nagle, R.B. (1996) Phrynosoma intraepidermal receptor: A dorsal intraepidermal mechanoreceptor in horned lizards (Phrynosoma; Phrynosomatidae; Reptilia). *Journal of Morphology*, 228(2), 145–154.

Sellers, K.C., Nieto, M.N., Degrange, F.J., Pol, D., Clark, J.M., Middleton, K.M. et al. (2022) The effects of skull flattening on suchian jaw muscle evolution. *The Anatomical Record*, 305, 2791–2822.

Stevens, M. (2013) *Sensory ecology, behaviour, and evolution*. Oxford, UK: Oxford University Press.

Stockdale, M.T. & Benton, M.J. (2021) Environmental drivers of body size evolution in crocodile-line archosaurs. *Communications Biology*, 4(1), 1–11.

Soares, D. (2002) Neurology: an ancient sensory organ in crocodilians. *Nature*, 417(6886), 241–242.

Thewissen, J.G. & Nummela, S. (Eds.) (2008) *Sensory evolution on the threshold: adaptations in secondarily aquatic vertebrates*. Berkeley, CA:University of California Press.

Turner, A.H., Pritchard, A.C. & Matzke, N.J. (2017) Empirical and Bayesian approaches to fossil-only divergence times: a study across three reptile clades. *PLoS One*, 12(2), e0169885.

Van Hemert, C., Handel, C.M., Blake, J.E., Swor, R.M. & O'Hara, T.M. (2012) Microanatomy of passerine hard-cornified tissues: Beak and claw structure of the black-capped chickadee (*Poecile atricapillus*). *Journal of Morphology*, 273(2), 226–240.

von Düring, M. (1973) The ultrastructure of lamellated mechanoreceptors in the skin of reptiles. *Zeitschrift für Anatomie und Entwicklungsgeschichte*, 143(1), 81–94.

Wang, S., Stiegler, J., Wu, P., Chuong, C.M., Hu, D., Balanoff, A. et al. (2017) Heterochronic truncation of odontogenesis in theropod dinosaurs provides insight into the macroevolution of avian beaks. *Proceedings of the National Academy of Sciences of the United States of America*, 114(41), 10930–10935.

Watkinson, G.B. (1906) The cranial nerves of *Varanus bivittatus*. *Gegenbaurs Morphologisches Jahrbuch*, 35, 450–472.

Wilberg, E.W. (2015) What's in an outgroup? The impact of outgroup choice on the phylogenetic position of Thalattosuchia (Crocodylomorpha) and the origin of Crocodyliformes. *Systematic Biology*, 64(4), 621–637.

Wilberg, E.W., Turner, A.H. & Brochu, C.A. (2019) Evolutionary structure and timing of major habitat shifts in Crocodylomorpha. *Scientific Reports*, 9(514), 1–10.

Willard, W.A. (1915) *The cranial nerves of* Anolis carolinensis. *Bulletin of the Museum of Comparative Zoology*, 59(2), 15–116.

Witmer, L.M. (1995) The extant phylogenetic bracket and the importance of reconstructing soft tissues in fossils. In: Thomason, J. (Ed.) *Functional morphology in vertebrate paleontology*. Cambridge, UK: Cambridge University Press, pp. 19–33.

Witmer, L.M., Ridgely, R.C., Dufeau, D.L. & Semones, M.C. (2008) Using CT to peer into the past: 3D visualization of the brain and ear regions of birds, crocodiles, and nonavian dinosaurs. In: *Anatomical imaging*. Tokyo: Springer, pp. 67–87.

Yi, H., Tennant, J.P., Young, M.T., Challands, T.J., Foffa, D., Hudson, J.D. et al. (2016) An unusual small-bodied crocodyliform from the Middle Jurassic of Scotland, UK, and potential evidence for an early diversification of advanced neosuchians. *Earth and Environmental Science Transactions of the Royal Society of Edinburgh*, 107(1), 1–12.

Yoshizawa, M. & Jeffery, W.R. (2011) Evolutionary tuning of an adaptive behavior requires enhancement of the neuromast sensory system. *Communicative & Integrative Biology*, 4(1), 89–91.

Young, B.A. & Wallach, V. (1998) Description of a papillate tactile organ in the Typhlopidae. *African Zoology*, 33(4), 249–253.

SUPPORTING INFORMATION

Additional supporting information can be found online in the Supporting Information section at the end of this article.

How to cite this article: Lessner, E.J., Dollman, K.N., Clark, J.M., Xu, X. & Holliday, C.M. (2023) Ecomorphological patterns in trigeminal canal branching among sauropsids reveal sensory shift in suchians. *Journal of Anatomy*, 242, 927–952. Available from: https://doi.org/10.1111/joa.13826